Effects of passive storage conceptualization on modelling hydrological function and isotope dynamics in the flow system of cockpit karst landscape

Guangxuan Li[1,2], Xi Chen[1,2*], Zhicai Zhang[3], Lichun Wang[1,2], Chris Soulsby[4]

Affiliations:

[1] Institute of Surface-Earth System Science, School of Earth System Science, Tianjin University, Tianjin, China, 300072

[2] Tianjin Key Laboratory of Earth Critical Zone Science and Sustainable Development in Bohai Rim

[3] College of Hydrology and Water Resources, Hohai University, Nanjing, China

[4] School of Geosciences, University of Aberdeen, Aberdeen AB24 3UF, United Kingdom

[*]**Correspondence to:** xi_chen@tju.edu.cn

Abstract

Conceptualising passive storage in coupled flow-isotope models can improve simulation of mixing and attenuation effects on tracer transport in many natural systems, such as catchments or rivers. However, the effectiveness of incorporating different conceptualisations of passive storage in models of complex karst flow systems remains poorly understood. In this study, we developed a coupled flow-isotope model that conceptualises both “fast” and “slow” flow processes in heterogeneous aquifers, in addition to hydrological connections between steep hillslopes and low-lying depression units in cockpit karst landscapes. The model tested contrasting configurations of passive storage in the fast and slow flow system and was optimized using a multi-objective optimization algorithm based on detailed observational data of discharge and isotope dynamics in the Chenqi catchment in southwest China. Results show that 1-3 passive storage zones distributed in hillslope fast/slow flow reservoir and/or depression slow flow reservoir provided optimal model structures in the study catchment. This optimization can effectively improve simulation accuracies for outlet discharge and isotope signatures. Additionally, the optimal tracer-aided model reflects dominant flow paths and connections of the hillslope and depression units, yielding reasonable source area apportionment for dominant hydrological components (e.g. more than ~80% of fast flow in the total discharge) and the solute transport in steep hillslope unit of karst flow systems. Our coupled flow-isotope model for karst systems provides a novel, flexible tool for more realistic catchment conceptualizations that can easily be transferred to other cockpit karst catchments.

Keywords: Flow-isotope model; passive storage; karst flow systems; Chenqi catchment; Hillslope and depression units

1 Introduction

Karst areas cover extensive areas of the Earth's surface providing important water resources. For example, the southwest China karst region is one of the world's largest continuous karst areas, covering ~540 × 10^3 km^2 over eight provinces and providing water resources for more than 100 million people (Chen et al., 2018). The strong dissolution of carbonate rocks in the humid tropics and subtropics of southwest China creates unique cockpit karst landscapes, covering an area of about 140,000 - 160,000 km2. Such cockpit karst morphology also occurs in areas in Southeast Asia, Central America and the Caribbean. In polje/tower karst systems, depression areas are interconnected with isolated towers scattered throughout the terrain (Lyew et al., 2007). Since hillslope runoff is regarded as a "water tower" often supplying agriculture in the depression, the development of hydrological models representing the hillslope and depression hydrological functionality is a necessary prerequisite for water resources management in cockpit karst landscapes.

A wide range of hydrological models have been developed for karst areas, ranging from lumped models at the catchment scale to (semi-) distributed models with hydrological function parameterized for grid-scales or landscape unit scales (Martínez‐Santos and Andreu, 2010; Hartmann et al., 2013; Husic et al., 2019; Dubois et al., 2020; Ollivier et al., 2020; Xu et al., 2020; Jeannin et al., 2021; Wunsch et al., 2022). A key function of karst hydrological models is to capture the dual or multi-phase flows in a complex porous medium, capturing low velocities in the matrix and small fractures, as well as very high velocities in large fractures and conduits (White, 2007;

Worthington, 2009; Jourde et al., 2018; Ding et al., 2020). Model structures endowed with process-based conceptualization of complex distributed flow systems often lead to over-parameterization and large uncertainties for resulting simulation (Perrin et al., 2001; Beven, 2006; Adinehvand et al., 2017). More generally, in recent years isotope-aided hydrological models have been developed to fully couple hydrological processes with stable isotope dynamics (Birkel and Soulsby, 2015). These coupled models are effective in quantifying hydrological functions, such as water storage, flux, and ages (Long and Putnam, 2004; Carey and Quinton, 2004; Delavau et al., 2017; Chacha et al., 2018; Zhang et al., 2020b; Elghawi et al., 2021; Mayer-Anhalt et al., 2022), which are useful metrics to characterize the karst critical zone and associated flow systems.

In isotope-aided hydrological models, flow routing is driven by pressure gradients, creating a dynamic (active) water storage that is influenced by water balance considerations (Fenicia et al., 2010; Soulsby et al., 2011), while tracer mixing, attenuation and transport require additional storage volumes (passive storage), such as unsaturated storage below field capacity (Birkel et al., 2011b) or saturated storage at depths far below the stream or water table. The conceptual combination of active storage with passive storage in isotope-aided hydrological models enhances solute mixing and resultant tracer retardation. As summarized in Table 1, previous tracer-aided hydrological models incorporate at least one passive storage. Generally, the number of passive storages increases with the sub-division of storage according to landscape units. For example, simple models with one (unsaturated/saturated or total) storage unit have one passive storage parameter (Barnes and Bonell., 1996; Fenicia et al., 2010; Ala-Aho et al., 2017). For more complex models with at least two geographical units of uplands and lowlands, the number of passive storages could increase to 2-5 (Birkel et al., 2011a; Capell et al., 2012; Birkel et al., 2015; Mayer-Anhalt et al., 2022). Although these studies have provided a useful proof of concept, assessment of alternative configurations of passive storage functions has rarely been systematically tested.

For the complex flow systems in cockpit karst landscapes, a few studies have recently incorporated passive storage into coupled flow-isotope models for simulating hydrological and solute transport processes. For example, Zhang et al. (2019) developed a semi-distributed conceptual model for capturing discharge and isotope dynamics in the Chenqi catchment. The model has a function for passive storage to affect isotope mixing only within a conceptual hillslope unit, but it did not incorporate any passive storages in fast and slow reservoirs in the depression unit. Chang et al. (2020) compared lumped model structures with different connections of epikarst and the underlying slow and fast reservoirs according to observations of spring discharge and electrical conductivity (EC) in the Yaji catchment of southwest China. They set a passive storage for the fast flow reservoir but neglected passive storage in the slow flow system. These previous model structures with only one passive storage (Zhang et al., 2019; Chang et al., 2020) may not always be sufficient to simulate the distributed functioning of chemical mixing between active and passive storages and the hillslope flow-depression flow inter-connections. Moreover, previous coupled models (listed in Table 1) are mostly calibrated and validated only against daily and/or weekly streamflow and isotope signatures. In karst catchments, as discharge responses and isotope concentrations can vary extremely rapidly, the coarse resolution field data cannot capture the hydrological and isotopic dynamics.

The overall aim of this study is to evaluate the effectiveness of alternative ways of incorporating passive storage into a generic coupled flow-isotope model for cockpit karst landscapes. The specific objectives were to: (1) develop a model that characterizes the functions of fast and slow flow paths from hillslope to depression units for water and tracer transport in cockpit karst landscapes; (2) systematically test alternative passive storage configurations into the generalized model structure using a multi-objective optimization algorithm based on detailed observational data of discharge and isotope dynamics in the Chenqi catchment of southwest China; and (3), identify the most appropriate model structures that most efficiently describe the hydrological functioning of the catchment in terms of simulating the stream flow and tracer responses.

Table 1. Summary of the previous studies that account for passive storages in hydrological models using at least one isotopic tracer

Scale	Model	Number of passive storages	Location of passive storages	Tracer	Function	References
25 ha	Models with fast and slow flow reservoirs	1	One storage	D	A	Barnes and Bonell., 1996
3.5 km^2	Chemical-mixing	2	Shallow and deep storages	Chloride	A and B	Page et al., 2007

	dynamic TOPMODEL					
23.6 km^2	The multiple bucket model	3	Soil storage	D	A	Son et al., 2007
3.8 ha	The SoftModel$_i$	2	Upper and lower hillslope storages	D	A	Fenicia et al., 2008
3.8 ha	Complete mixing and partial-mixing model	1	One storage	D	B	Fenicia et al., 2010
2.3 and 122 km^2	Lunan-CIM (L-CIM)	2-5	2 for upper and low storages in upper catchment, and 3 for upper, low and deep storages in lower catchment	D	A	Birkel et al., 2011a
3.6 and 30.4 km^2	SAM^{dyn} model	1	The total catchment storages	^{18}O	C	Birkel et al., 2011b
749 km^2	The tracer-aided model	4	Shallow and deep storages for uplands and lowlands	D and alkalinity	A	Capell et al., 2012
1.4, 8 and 9.6 km^2	The DYNAMIT (DYNAmic MIxing Tank)	2	Unsaturated zone and slow flow reservoir	Chloride	A and B	Hrachowitz et al., 2013
30 km^2	Tracer-aided hydrological model for a wet Scottish upland catchment	3	Three storages (upper, lower and saturation areas)	^{18}O	B and C	Birkel et al, 2015
3.7 km^2	Hydrochemical model of Upper Hafren	2	Shallow and groundwater storage	Chloride	A and B	Benettin et al., 2015
3.2 km^2	The landscape-based dynamic model	3	Three storages (hillslope, groundwater, and saturation area)	D	B	Soulsby et al., 2015
3.2 km^2	STARR (Spatially Distributed	2	Soil and groundwater storage	D	A, B and C	van Huijgevoort et al., 2016

3.2, 0.6 and 0.5 km^2	Tracer-Aided Rainfall-Runoff model) STARR (Spatially Distributed Tracer-Aided Rainfall-Runoff model)	1	Soil storage	^{18}O	A and B	Ala-Aho et al., 2017
3.2 km^2	STARR model for the humid tropics	2	Soil and groundwater storage	D	A and C	Dehaspe et al., 2018
10.2 ha	A conceptual catchment model	2	Shallow and groundwater storage	^{18}O	A, B and C	Rodriguez., 2018
1.25 km^2*	Tracer-aided hydrological model for karst	1	Hillslope storage	D	A, B and C	Zhang et al., 2019
7.8 km^2	STARR (Spatially Distributed Tracer-Aided Rainfall-Runoff model)	2	Soil and groundwater storage	D	A, B and C	Piovano et al., 2019
3.2 km^2	A tracer-aided hydrological model	3	Dynamic hillslope reservoir, dynamic riparian zone reservoir and groundwater reservoir	D	A	Neill et al., 2019
126 km^2	A coupled, tracer-aided, conceptual rainfall-runoff model	4	Four storages (upper, lower and saturation areas and deep groundwater)	D and dissolved organic carbon	A and B	Birkel et al., 2020
Spring*	Lumped Model for karst	1	Fast flow reservoir	EC	A	Chang et al., 2020
0.23, 0.5, 0.6, 3.2 and 7.8 km^2	A spatially distributed tracer-aided hydrological	1	Soil storage	D and ^{18}O	A, B and C	Piovano et al., 2020

	model (STARR)					
1.44 km^2	The EcH_2O-iso Model	1	The extra groundwater storage	D and ^{18}O	A, B and C	Yang et al., 2021
3.9 km^2	A conceptual tracer-aided hydrological model	3	The upper, lower and groundwater storages	D	A and B	Mayer-Anhalt et al., 2022
0.9 km^2*	The coupled flow-isotope model for karst catchment	2	Slow and fast flow reservoirs in hillslope and depression units	D	A and C	This study

Note: A represents that passive storage can help reproduce the main isotope dynamics and improve simulation accuracy; B represents that passive storage can help track flux, resident or transit time; C represents that passive storage can help estimate catchment storage. D is the abbreviation for deuterium. *refers to application in a karst catchment.

2 Study area and data descriptions

2.1 Study area

Chenqi is a small karst catchment located in the Puding Karst Ecohydrological Observation Station, Guizhou Province of southwest China (Fig. 1). Chenqi belongs to the subtropical monsoon climate zone with a mean annual temperature of 14.2℃, mean annual rainfall of 1140 mm, and mean annual humidity of 78%. Precipitation mainly occurs in the rainfall season (May-August), accounting for more than 80% of the annual amount. The catchment is a typical karst peak cluster landform where a central depression is surrounded by hillslopes with elevations ranging from 1340m to 1530m. Considering the distinct topographic features, the catchment is conveniently divided into two dominant geomorphic units: hillslope and depression, with an area of 0.73 and 0.17 km^2, respectively (Table 2). Due to the peak cluster depression landform, runoff generated from hillslopes mostly flows into depression aquifer prior to contributing to streamflow at the catchment outlet (Zhang et al., 2019; Zhang et al., 2020a).

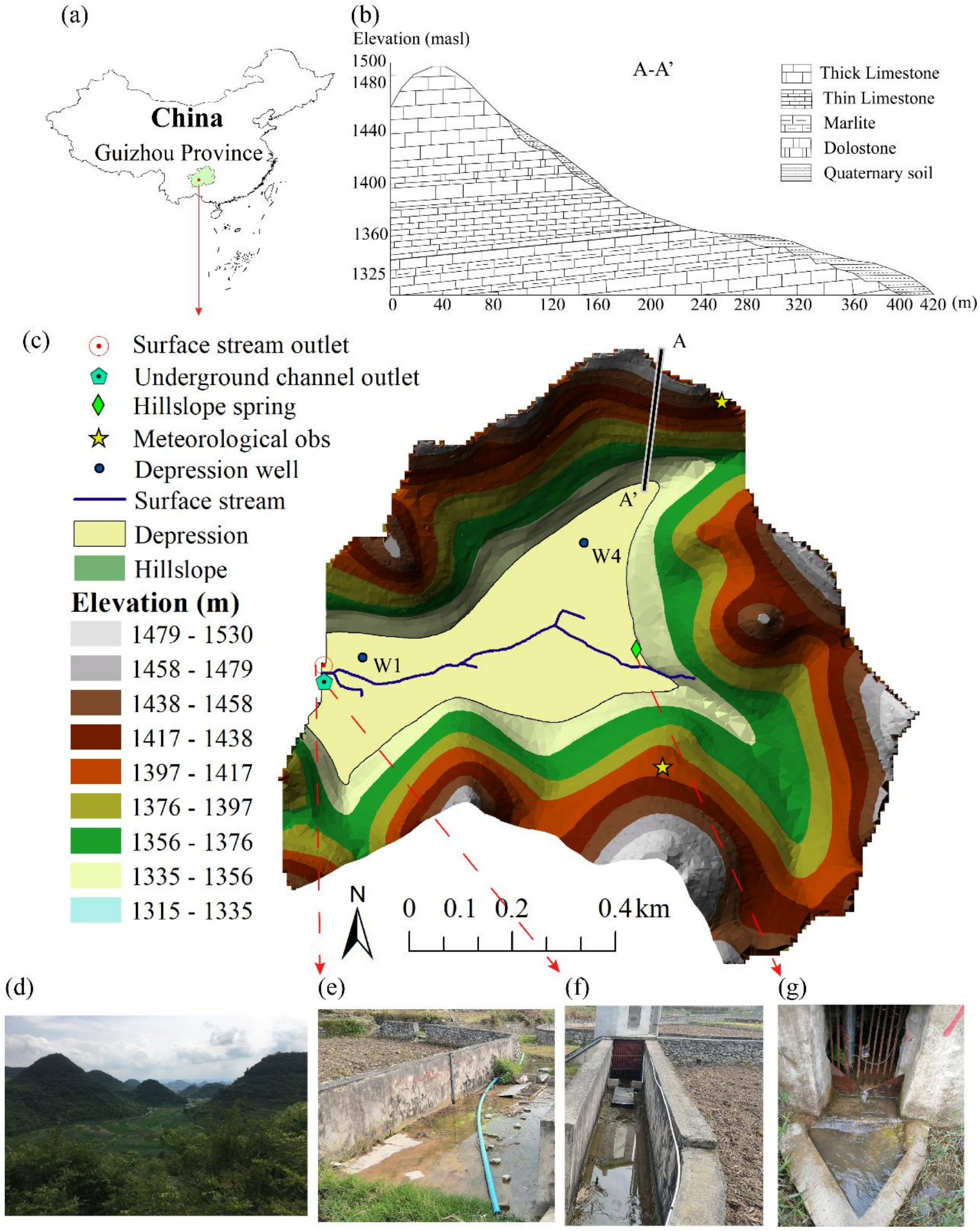

Figure 1. The location of Chenqi catchment (a), stratigraphic profile (b), topography (c), photo (d), and observations at surface stream outlet (e), underground channel outlet (f) and hillslope spring (g).

Table 2. The catchment characteristics of two landscape units at Chenqi

	Hillslope	Depression
Area (km^2)	0.73	0.17

Elevation (m.a.s.l.)	1340-1530	1315-1340
Soil thickness	＜0.5 m	＞2 m
Land cover and use	Forest (13.67%), shrub (30.38%), grass (12.26％) and crops (40.1%)	

2.2 Hydrogeological properties

Geological characteristics of the catchment include Quaternary soil, thick and thin limestone, dolostone, and marlite. The limestone formations with a thickness of 150-200 m lie above an impervious marlite formation (see A-A' profile in Fig. 1b) (Chen et al., 2018). In hillslopes, field investigations have shown a rich fracture zone (epikarst) which has a thickness of 7.5-12.6 m (Zhang et al., 2011). Quaternary soils consist of mostly sand (56-80%), fine sand (20-40%), calcareous soil and silt (1-10%). The soils are thin (less than 30 cm) and irregularly developed on carbonate rocks. Outcrops of carbonate rocks cover 10%-30% of the hillslope area. In some specific areas where a shallow impermeable layer (marlite) exists, hillslope springs appear on lower hillslopes. Deciduous broadleaved forests and shrubs are mostly grown on the upper and middle parts of hillslopes, and corn is grown at the foot of the gentle hillslopes (Chen et al., 2018).

In the low-lying depression, the accumulated soils are thicker (~2 m) and cultivated for crops of corn and rice paddy. The underlying limestone is strongly dissolved, producing underground conduits. These are sporadically distributed in the upper depression areas in connection with hillslope flows, and are gradually concentrated towards the catchment outlet (Cheng et al., 2019). The bedrock comprising the impervious marlite is located at depths of 30-50 m. Meanwhile, there are depression ditches used for draining flood flow when the groundwater level is higher than the ditch bottom (see surface stream in Fig. 1). So, the total outlet discharge is composed predominantly of underground conduit flow in the study catchment, with surface channel flow only in larger events.

2.3 Observational dataset of hydrometry and stable isotope

In the Chenqi catchment, an automatic meteorological station (Fig. 1c) was installed to continuously record rainfall, temperature, air pressure, wind speed, humidity, and solar radiation. These data were used to calculate the potential evaporation via the Penman formula. Discharge at hillslope springs and the catchment outlet were measured by v-notch weirs with a time interval of 15 min. All observational datasets were collected from 8 October 2016 to 12 June 2018.

For stable isotope analysis, the hillslope springs, the catchment outlet flows, and rainfall were sampled using an autosampler set. The sampling frequency was daily in dry season (September - April) and hourly in the rainy season (May - August). In total, we collected 253 rainfall samples, 1095 hillslope spring samples and 1096 water samples at the catchment outlet of underground channel during the study period (Table 3).

As shown in Fig. 1c, there are two observation wells (W1 and W4) near the catchment outlet and the upstream depression. W1 is located in a local confined aquifer surrounded by rocks with poor permeability, and W4 is located in a high permeability zone (Chen et al., 2018). The depression groundwater in the two wells (W1 and W4 in Fig. 1c) was manually sampled. Samples were taken at depths of 35 m and 13 m for

W1 and W4, respectively, with a sampling frequency of two occasions before and after the four rainfall events from 6 July 2017 to 20 August 2017.

The sampled water was sealed by using plastic bags to avoid evaporation. Water samples were taken to the laboratory every day and stored at about 4 ℃. The water samples were tested and analyzed by the MAT 253 laser isotope analyser (instrument precision was ± 0.5 ‰ for δD and ± 0.1 ‰ for $\delta^{18}O$) at the State Key Laboratory of Hydrology and Water Resources of Hohai University.

2.4 Characteristics of the observed hydrograph and stable isotope dynamics

The observed surface, subsurface and total outlet flow (discharge) are shown in Fig. 2. The discharge response to rainfall is rapid, characterized by a sharp rise and decline of hydrographs. During the study period, the surface flow and underground flow are 43% and 57% of the total discharge, respectively. Various lines of evidence have demonstrated the hillslope-depression fast flow connection, particularly during heavy rainfall events. In the mid-season, after extremely heavy rainfall, hillslope flow is highly synchronized with outlet flow, and the relationship between hillslope spring discharge and outlet discharge approaches a monotonic function (details in Zhang et al., 2020a). It is worth noting that due to the impact of agricultural irrigation, there were unreasonable sudden declines in surface and subsurface flow in June.

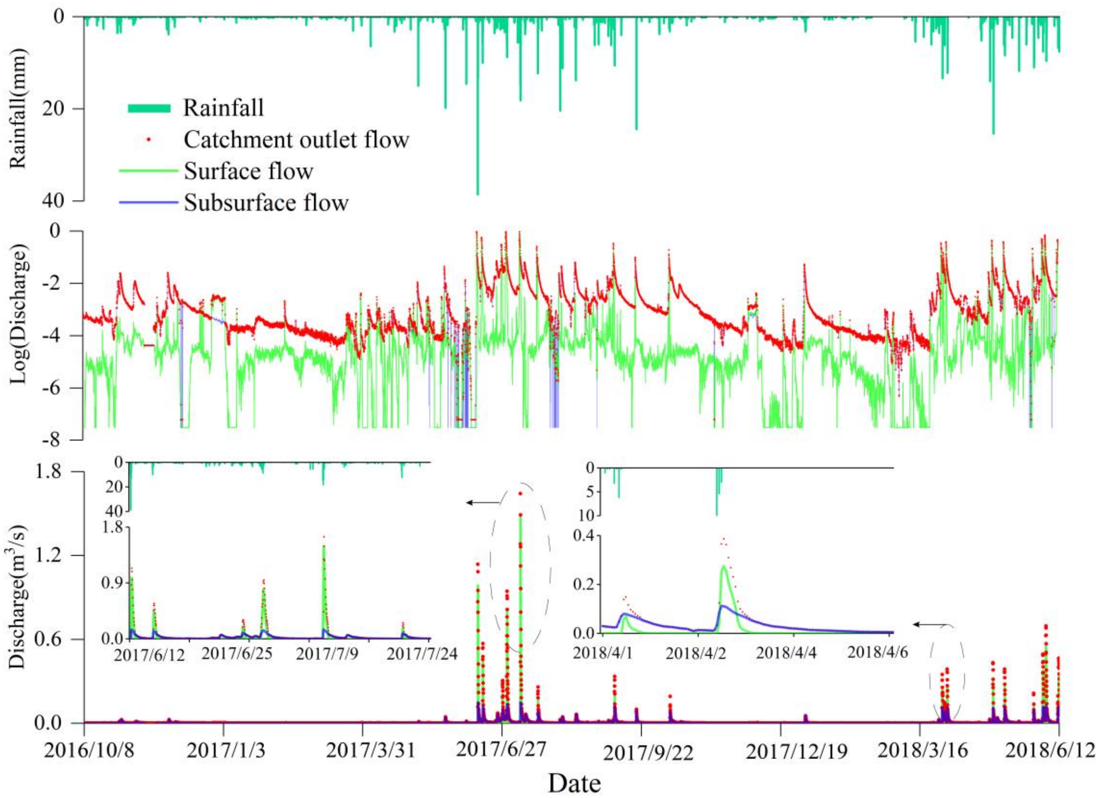

Figure 2. The observed surface, subsurface and catchment total outlet flow (discharge) during the study period.

The mean values of δD and $\delta^{18}O$ (Table 3) clearly show that the isotopic composition of water in the catchment becomes more enriched from the hillslope spring to the depression groundwater and the catchment outlet discharge. This implies increased mixing with more enriched groundwater affected by evaporative fractionation over the course of water flow paths from the hillslopes towards the outlet (Zhang et al., 2019; Zhang et al., 2020a). When plotted in dual isotope space, the data points of the δD - $\delta^{18}O$ regression line for the hillslope spring and outlet discharge are shown in Fig. 3. This also illustrates that the hillslope and depression flows undergo evaporative effects as their regression lines deviate the LMWL ($\delta D = 8.18\delta^{18}O + 9.52$). Additionally, the regression line of hillslope flow is close to that of the catchment outlet discharge, inferring that hillslope flow is a primary source of the outlet discharge. In depression, the isotopic concentration of groundwater flow at W1 and W4 is quite different. W1 is located in the less permeable area and flow there seldom mixes with new water (rainfall), resulting in more enriched δ^{18}O and δD values. By contrast, W4 is located in the high permeability zone and groundwater there receives more new water (fast flow) from the hillslope spring and rainfall, resulting in more depleted isotope signals (Chen et al., 2018).

The monthly statistical summaries of δD and lc-excess (lc-excess=δD-a·δ^{18}O-β) are shown in Fig. 4. In the wet season from May to October, the δD is gradually depleted, reflecting rainfall inputs, while in the dry season from November to April, the δD is gradually enriched. It indicates that both the hillslope spring and outlet discharge change from receiving more new rain water in wet season to being dominated by older water in the dry season. Meanwhile, the δD is more depleted and the lc-excess is more positive for the hillslope flow, compared to the outlet discharge. It means that additional flow sources in the depression join the hillslope flow. This depression flow is older but undergoes less evaporation because of the flat topography and thicker soils. Nevertheless, the additional depression flow has little influence on discharge variability at the catchment outlet, as the various patterns of δD and lc-excess at catchment outlet closely correspond to those of the hillslope spring.

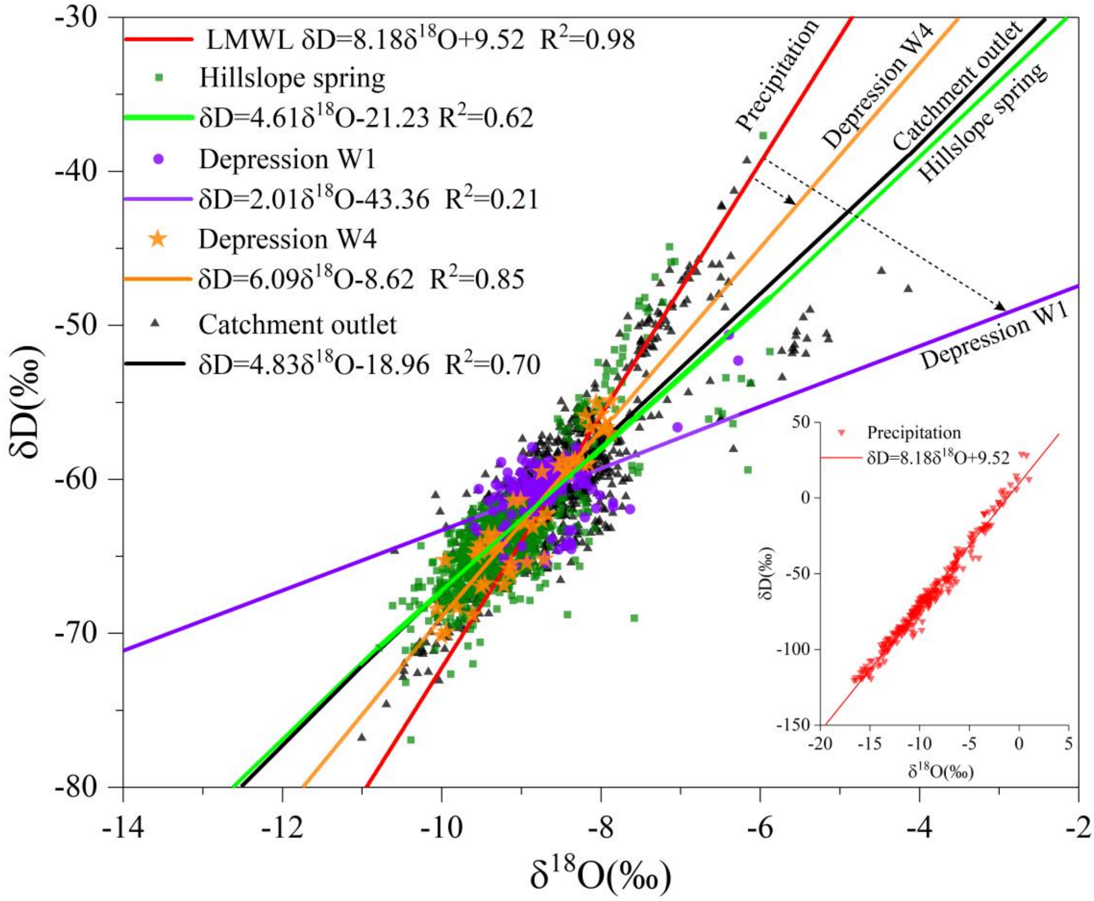

Figure 3. Plot of $\delta^{18}O$-δD for rainwater, catchment outlet discharge, hillslope spring and depression groundwater at wells W1 and W4. The correlation between $\delta^{18}O$ and δD at W1 is 0.21, and tested to be significant at the significance level of p<0.001.

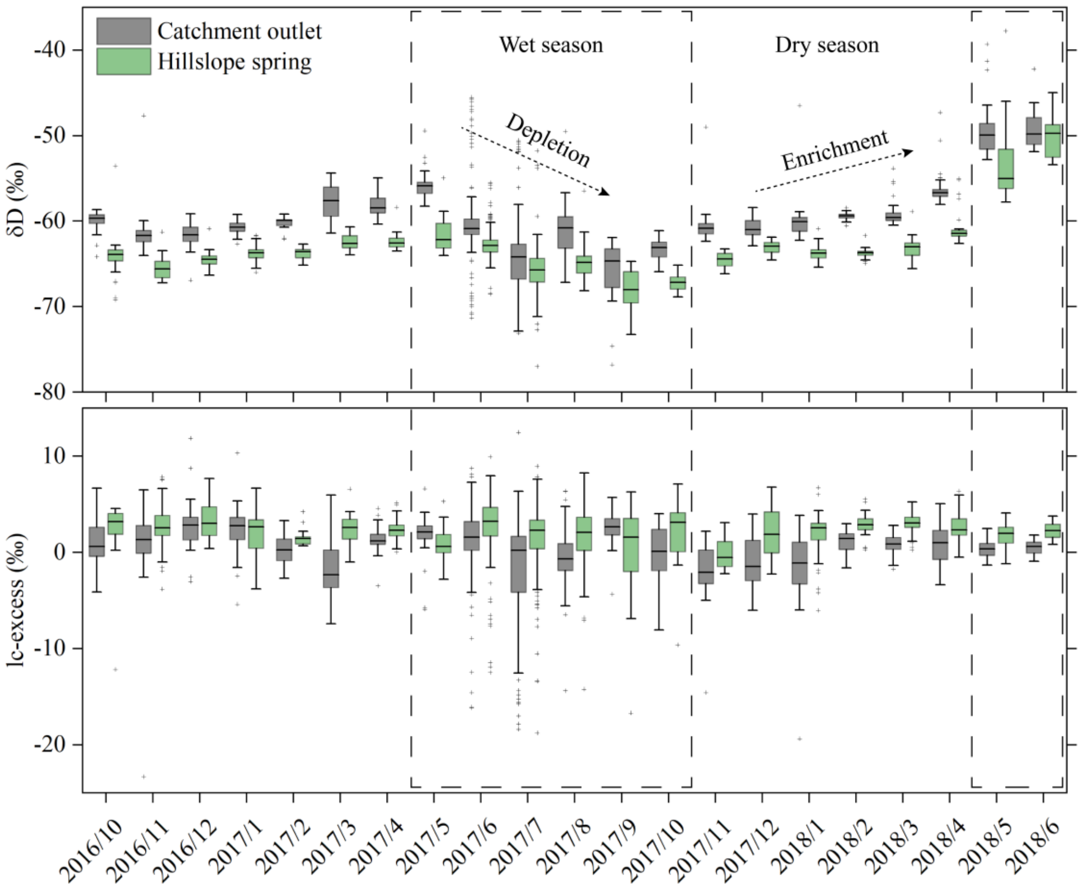

Figure 4. Monthly summaries of observed δD and lc-excess of outlet discharge and hillslope spring during the study period.

Table 3. Statistical characteristics of isotope data for rainfall, hillslope spring, catchment outlet discharge and depression groundwater in the study period

Obs	Sampling time	Number	δD (‰)			$\delta^{18}O$ (‰)			lc-excess	
			Range	Mean	CV	Range	Mean	CV	Range	Mean
Rainfall		253	-120.2-29	-64.9	0.49	-16.6-1.0	-9.1	0.42	-16.71-17.37	-0.04
Catchment outlet discharge	Oct. 8 2016 - June 12 2018	1096	-76.8- -39.3	-60.6	0.07	-11- -4.1	-8.6	0.09	-23.31-12.45	0.33
Hillslope spring		1095	-77- -37.8	-63.7	0.05	-10.8- -5.9	-9.2	0.06	-18.77-9.92	2.06
Groundwater W1	July 6- Aug. 20, 2017	175	-65.7- -50.7	-60.8	0.03	-9.6- -6.3	-8.7	0.05	-10.75-7.6	0.65
Groundwater W4	July 6- Aug. 20, 2017	47	-70.2- -55	-62.5	0.07	-10.1- -7.9	-8.9	0.07	-3.56-6.51	0.96

3 Model development

3.1 Conceptual model structure

Considering the contrasting features of the catchment landscape, the catchment area is conveniently sub-divided into hillslope and depression units, and the model structure can be conceptualized by focusing on the hydrologic connectivity of the "hillslope-depression-stream" continuum (Zhang et al., 2020a). In each of hillslope and depression units, the vertical profile is separated into an unsaturated zone comprising the soil and epikarst layers, and a saturated zone representing the deep aquifer (Fig. 5). The effect of spatial heterogeneity on hydrological functions is described by a distribution curve of storage in the unsaturated, and a dual flow system in the saturated zone. The distribution curve of storage, like a set of compartments in the VarKarst model (Hartmann et al., 2013), has functions to quantify various recharge mechanisms (e.g., diffusive and concentrated allogenic and autogenic recharge). The dual flow system consists of a fast flow reservoir and a slow flow reservoir that are interconnected and can be used for groundwater routing (Hartmann et al., 2013; Zhang et al., 2019).

The steep hillslope flow moves to the low-lying depression with the following possible connections: hillslope fast flow to depression fast/slow flow (HF-DF/DS), and hillslope slow flow (HS) to depression fast/slow flow (Fig. 5). As hillslope fast flow is primarily concentrated into depression conduits, the connection of HF-DS is neglected in this study.

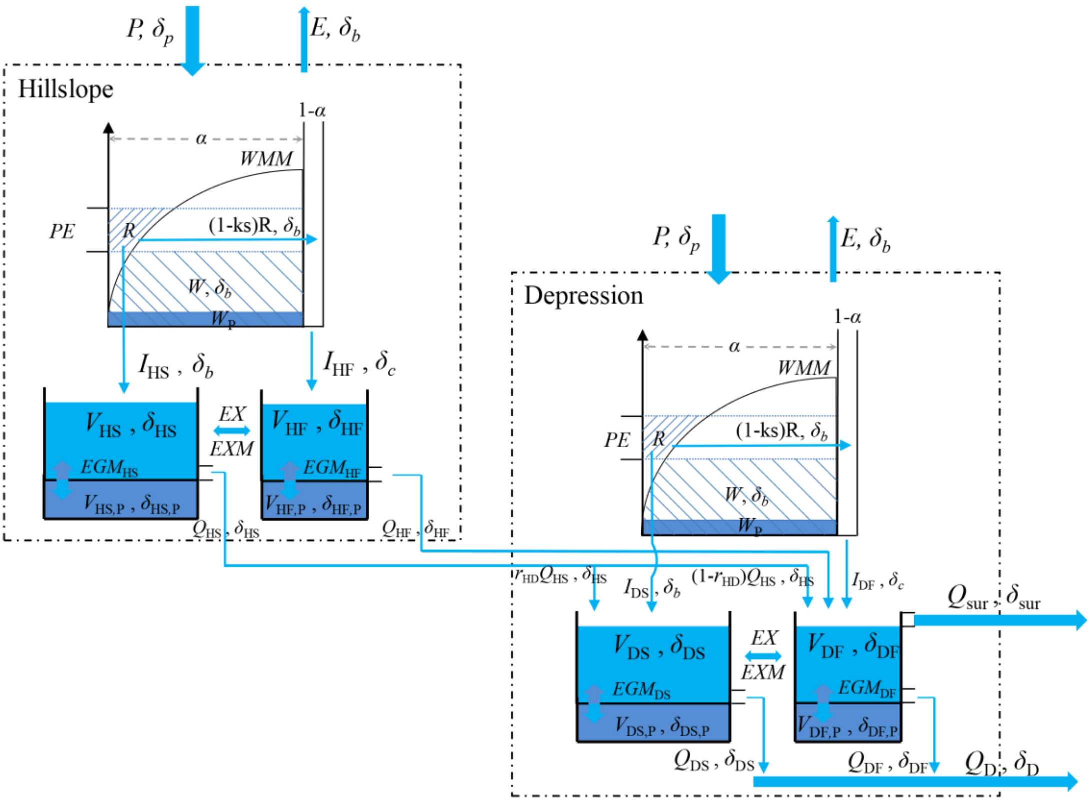

Figure 5. Conceptualized structure for the coupled flow-isotope model. The light blue shades indicate active storage, the dark blue shades indicate passive storage. The detailed descriptions of the model parameters are shown in Table 5.

3.1.1 Hydrological routing

In each of hillslope and depression units, the spatial heterogeneity of unsaturated storage volumes is described by a distribution curve of the storage capacity like the Xinanjiang model in Fig. 5 (Zhao, 1992) following:

$$\frac{f}{F} = 1 - (1 - \frac{wm'}{WMM})^b \qquad (1)$$

where f represents free water yield area, F represents the total of the area (α), wm' is the areal mean tension water storage at f, WMM is the maximum value of wm', and b is a parameter.

Based on Eq. (1), the initial areal average storage W is an integration of wm' within 0-A in the area (1-f/F) :

$$W = \int_0^A (1-\frac{wm'}{WMM})^b dwm' = \frac{WMM}{1+b}\left[(1-\frac{A}{WMM})^{1+b}\right] \tag{2}$$

when A=WMM, the storage in the entire area reaches the storage capacity. Thus, the mean storage capacity wm is equal to $\frac{WMM}{1+b}$ (Zhao, 1992).

When the net precipitation PE (PE=P-E)>0 and if P-E+A<WMM, the water yield R is:

$$R = P - E - wm + W + wm(1-\frac{P-E+A}{WMM})^{1+b} \tag{3}$$

Note that P is precipitation and E is actual evaporation estimated by $E = kc \times Ep \times \frac{W}{wm}$, in which kc is a coefficient for evapotranspiration, and Ep is potential evapotranspiration.

If P-E+A≥WMM, the water yield R is:

$$R = P - E - wm + W \tag{4}$$

The water yield R recharges the deep aquifer, which is separated into diffusive recharge I_S and concentrated allogenic and autogenic recharge I_F. The I_S recharges the slow flow reservoir of the matrix or small fracture area with a ratio to hillslope or depression area of α (i.e., I_S=ks×R×α, where ks is the ratio of water yield into slow flow reservoir). The I_F is the remaining runoff ((1-ks)×I_S) and rainfall P falling on the swallow holes (1-α), which directly recharges fast flow reservoir (i.e., I_F=P×(1-α)+R×(1-ks)×α).

Consequently, in the saturated zone, the water balance in the fast and slow reservoirs is:

$$\frac{dV_S}{dt} = I_S - EX - Q_S \tag{5}$$

$$\frac{dV_F}{dt} = I_F + EX - Q_F \tag{6}$$

where V_S and V_F are storages of the slow and fast flow reservoirs, respectively; Q_S and Q_F are discharges from the slow and fast reservoirs, respectively; EX is flux between fast flow and slow flow reservoirs.

EX is estimated by difference of the saturated storages (or water heads) between the fast flow and slow flow reservoirs (i.e., $EX=ke\times(V_S-V_F)$), where ke is a coefficient of exchange flux between the slow and fast flow reservoirs). Q_S and Q_F are estimated according to the linear relationship between storage V and discharge (i.e., $Q_S=\eta s\times V_S$, and $Q_F = \eta f\times V_F$, where ηs and ηf are outflow coefficients of slow and fast flow reservoirs, respectively).

3.1.2 Isotopic tracer routing

In each of the hillslope and depression units, the isotope mass balance in the unsaturated zone storage can be expressed as:

$$\frac{d(WU\delta_b)}{dt} = P\delta_p - R\delta_b - E(1+ls)\delta_b \tag{7}$$

where WU ($WU=W+W_P$) is the moisture storage consisting of active storage W or mobile water (Sprenger et al., 2017; Sprenger et al., 2018) and passive storage W_P, ls is the coefficient of evaporation fractionation, δ_p and δ_b are the stable isotope ratios of rainwater (P) and moisture (and water yield R), respectively. Eq. (7) assumes instantaneous mixing of rainwater (P), water yield (R) and soil moisture (W), and complete mixing of the active storage (W) with passive storage (W_P) in the area (α) since soils are very thin.

For the deeper aquifer, the mass balance in the slow and fast flow reservoirs is given by:

$$\frac{d(V_{\mathrm{S}}\delta_{\mathrm{S}})}{dt} = I_{\mathrm{S}}\delta_b - EXM - EGM_{\mathrm{S}} - Q_{\mathrm{S}}\delta_{\mathrm{S}} \tag{8}$$

$$\frac{\mathrm{d}(V_{\mathrm{F}}\delta_{\mathrm{F}})}{dt} = I_{\mathrm{F}}\delta_c + EXM - EGM_{\mathrm{F}} - Q_{\mathrm{F}}\delta_{\mathrm{F}} \tag{9}$$

where *EXM* is the exchange mass between the slow flow and fast flow reservoirs (estimated by $ke\times(V_{\mathrm{S}} - V_{\mathrm{F}})\times\delta_{\mathrm{S}}$ for $EXM>0$, and $ke\times(V_{\mathrm{S}} - V_{\mathrm{F}})\times\delta_{\mathrm{F}}$ for $EXM<=0$); EGM_{S} and EGM_{F} represent the mixing of the solute between the active and passive storages for the slow and fast flow reservoirs, respectively; δ_{S} and δ_{F} are the stable isotope δ of the slow flow and fast flow, respectively.

Since I_{F} comes from percolation of both unsaturated zone and direct rainfall recharge, the recharge water mass $I_{\mathrm{F}}\delta_{\mathrm{c}}$ is equal to

$$I_{\mathrm{F}}\delta_c = P\delta_p(1-\alpha) + \delta_b R(1-ks)\alpha \tag{10}$$

The mass balance of the passive storage ($V_{\mathrm{P}}\,\delta$) affected by EGM_{S} and EGM_{F} for slow and fast flow reservoirs is:

$$\frac{d(V_{\mathrm{S,P}}\delta_{\mathrm{S,P}})}{dt} = EGM_{\mathrm{S}} \tag{11}$$

$$\frac{d(V_{\mathrm{F,P}}\delta_{\mathrm{F,P}})}{dt} = EGM_{\mathrm{F}} \tag{12}$$

where $V_{\mathrm{S,P}}$ and $V_{\mathrm{F,P}}$ are the passive storage of slow flow and fast flow reservoirs, respectively; $\delta_{\mathrm{S,P}}$ and $\delta_{\mathrm{F,P}}$ are the stable isotope δ of passive storage for the slow flow and fast flow reservoirs, respectively; $EGM_{\mathrm{S}} = \varphi_{\mathrm{S}}\times V_{\mathrm{S}}\times(\delta_{\mathrm{S}} - \delta_{\mathrm{S,P}})$ and $EGM_{\mathrm{F}} = \varphi_{\mathrm{F}}\times V_{\mathrm{F}}\times(\delta_{\mathrm{F}} - \delta_{\mathrm{F,P}})$, where φ_{S} and φ_{F} are the exchange coefficient between the active and passive storages for slow flow and fast flow, respectively.

The above Eqs. (8) and (11) describe partial mixing between V_S and $V_{S,P}$ for the slow flow reservoir, and Eqs. (9) and (12) describe partial mixing between V_F and $V_{F,P}$ for the fast flow reservoir. Moreover, the partial mixing could be static or dynamic depending on whether the exchange coefficients between active and passive storages (φ_S and φ_F) are constant or vary over time, respectively (Hrachowitz et al., 2013).

3.1.3 Hillslope - depression connectivity and schematic model structures incorporating passive storage

The hillslope fast flow is assumed to fully connect with fast pathways in depression (i.e., HF-DF in Table 4) while the hillslope slow flow passes through both the slow matrix and fast pathways in the depression (i.e., HF-DF/DS in Table 4). Therefore, the storages of V_S and V_F in the depression unit receive additional recharge from the hillslope slow flow. So, the hillslope slow/fast flow contribute to the depression slow/fast flow is $r_{HD}\frac{A_H}{A_D}Q_S$ and $(1-r_{HD})\frac{A_H}{A_D}Q_S+\frac{A_H}{A_D}Q_F$, respectively, where r_{HD} is a ratio of hillslope slow flow into depression slow flow, A_H and A_D are hillslope and depression areas, respectively. Correspondingly, $V_S\delta_S$ and $V_F\delta_F$ in the depression are influenced by the isotope composition of the hillslope inputs ($r_{HD}\frac{A_H}{A_D}Q_S\delta_S$ and $(1-r_{HD})\frac{A_H}{A_D}Q_S\delta_S+\frac{A_H}{A_D}Q_F\delta_F$ from the hillslope slow flow and fast flow, respectively).

There is a dual drainage system comprising both a surface stream and underground channel in the depression. Here, we set a critical volume V_m in the depression. The catchment flow drains from surface stream Q_{sur} only when the depression groundwater storage meets: $V_{DF} > V_m$ (i.e., $Q_{sur} = \frac{(V_{DF} - V_m) \times A_D}{\Delta t}$). As a consequence, the total flow discharge at the catchment outlet Q is composed of fast flow (Q_F) and slow flow (Q_S) in the subsurface, with additional contribution from the surface stream Q_{sur}.

The passive storage may exist in any flow systems (fast and slow flow) and geographical units (hillslope and depression) in karst catchments (Fig. 5). To optimize the number and positions of passive storage in the flow system, we set fourteen schemes (scenarios) that incorporates 0-4 passive storages into different positions of fast and slow reservoirs for hillslope and depression units (indicated by the subscript P in Table 4). The model parameters and their definitions are listed in Table 5.

Table 4. Different model structures that incorporate passive storages into fast flow and/or slow flow reservoirs at hillslope and/or depression units

No. of Passive Storage	Model	Passive storage in hillslope		Passive storage in depression		Connection of flow system
		Slow flow (HS)	Fast flow (HF)	Slow flow (DS)	Fast flow (DF)	
0	*a*	-	-	-	-	HF-DF and HS-DS/DF
1	*b*	P	-	-	-	HF-DF and HS_P-DS/DF
	c	-	P	-	-	HF_P-DF and HS-DS/DF
	d	-	-	P	-	HF-DF and HS-DS_P/DF
	e	-	-	-	P	HF-DF_P and HS-DS/DF_P
2	*f*	P	P	-	-	HF_P-DF and HS_P-DS/DF
	g	-	-	P	P	HF-DF_P and HS-DS_P/DF_P
	h	P	-	P	-	HF-DF and HS_P-DS_P/DF
	i	-	P	-	P	HF_P-DF_P and HS-DS/DF_P
3	*j*	P	P	P	-	HF_P-DF and HS_P-DS_P/DF
	k	P	P	-	P	HF_P-DF_P and HS_P-DS/DF_P
	l	-	P	P	P	HF_P-DF_P and HS-DS_P/DF_P
	m	P	-	P	P	HF-DF_P and HS_P-DS_P/DF_P

4	*n*	P	P	P	P	HF_P-DF_P and HS_P-DS_P/DF_P

Note: The “P” and “-” represent the fast and slow flow reservoirs with and without passive storage, respectively.

3.2 Model calibration and validation

The observational data were used separately for the calibration and validation periods. That is, the model parameters were calibrated against the observed discharge and isotope concentration (δD) from October 8, 2016 to October 30, 2017. Afterwards, the model was validated against observations from November 1, 2017 to June 14, 2018. Note that since δD and $\delta^{18}O$ fluctuated with virtually the same dynamic over time and both were driven by the same hydrological factors, therefore only δD was used for calibration. The flow-isotope coupled models with different combinations of the active and passive storages (Table 4) were run on hourly time steps.

In this study, the multi-objective optimization algorithm, i.e., non-dominated sorting genetic algorithm II (NSGA-II) proposed by Deb et al (2002), was applied for the model parameter calibration. The NSGA-II algorithm (Kollat and Reed, 2006) based on NSGA algorithm can identify the sets of pareto-optimal solutions. As pareto-optimal sets of solutions are not dominated by any one of the factors as a result of trade-off effects, the “best” solution is achieved by satisfying the demands from the performance objective functions including the modified Kling-Gupta efficiency (KGE) and the absolute value of BIAS ($Abias_q$) (Fenicia et al., 2007). KGE criterion comprehensively considers the linear correlation and standard deviation between the numerical and observed values (Kling et al., 2012) following:

$$KGE_i = 1 - \sqrt{(r-1)^2 + (std-1)^2 + (\mu-1)^2} \tag{13}$$

where r is the linear correlation coefficient between the simulated and observed values, std is the ratio of the standard deviation of the numerical and observed values, and μ is the ratio of the average numerical value to the observed value, i = (q, c) representing the goodness of match for flow discharge or isotope concentration, respectively. The closer KGE is to 1, the better the overall performance of the coupled model.

The Abias_q is

$$\text{Abias}_q = \left| \frac{\sum_{i=1}^{n}(S_i - O_i)}{O_i} \right| \tag{14}$$

where S_i is the simulated discharge, and O_i is the observed discharge. The closer Abias_q is to 0, the better performance of model in matching flow discharge at the outlet.

For a number of iterations (e.g. 1000 in this study), 50 parameter sets were initially retained. Then the remaining sets with Bias_q less than or equal to 0.2 in the 50 parameter sets, are sorted from the largest to the smallest according to the sum of corresponding KGE_q and KGE_c. Finally, 30 sets are selected as the Pareto-optimal solution (Nan et al., 2021). The corresponding objective function values (average of the optimal solution sets) for both the calibration and validation periods were extracted.

The range of each parameter value is initially set for model calibration according to our previous investigations (Zhang et al., 2019; Zhang et al., 2020a; Xue et al., 2019). The volumes of passive storages ($W_{H,P}$ and $W_{D,P}$; $V_{S,P}$ and $V_{F,P}$) are generally one order of magnitude larger than those of active storage (Dunn et al., 2010; Soulsby et al., 2011;

Ala-Aho et al, 2017). So the ranges of $W_{H,P}$ and $W_{D,P}$ in the unsaturated zone are set as 500-550mm, and the ranges of $V_{H,P}$ and $V_{D,P}$ in saturated zone are set as 300-350mm. Considering the rapid hydrological response of the fast flow system or hillslope unit to precipitation, the initial values of active storage (V_{HF}, V_{DF} and V_{HS}) are set as 0 mm, while the initial value of V_{DS} is 20 mm (Xue et al., 2019). Meanwhile, the isotope ratios for deuterium are all initially set to the measurement at the catchment outlet (i.e., -61.3‰), this initialisation brings negligible errors since isotope transport is driven by rainfall inputs boundary condition.

A regional sensitivity analysis (Freer et al., 1996) was executed to identify the most important model parameters. The sensitive parameters targeting KGE_q are the ratio of water yield into slow flow reservoir (ks_H/ks_D), the maximum storage of the fast flow reservoir V_m, and the outflow coefficient of fast flow reservoir in hillslope unit (ηf_H). There are other sensitive parameters when targeting on KGE_c, including α_H, kc_H, ks_H, b_H, wm_H and ηs_H in the hillslope unit, and α_D, kc_D, and ηs_D in the depression unit. Overall, the parameters in the hillslope unit are more sensitive to discharge and isotopic ratios, compared with those in the depression unit.

Table 5. The definitions of model parameters with their ranges

Zone	Parameter and meaning		Range
Area	α_H/α_D	Ratio of matrix flow area	0.90-0.95/0.95-1
Unsaturated	kc_H/kc_D	Coefficient for evapotranspiration	0.9-1.3
	ks_H/ks_D	Ratio of water yield into slow flow reservoir	0.1-0.5
	b_H/b_D	Exponential distribution of tension water capacity	0.1-0.3

	ls_H/ls_D	coefficient of evaporation fractionation	0-0.1
	wm_H/wm_D	Tension water storage capacity (mm)	40-60/70-90
	$\#W_{H,P}/W_{D,P}$	passive storage (mm)	500-550
Saturated	-/Vm	Maximum storage of fast flow reservoir (mm)	30-50
	r_{HD}	Ratio of hillslope slow flow into slow flow reservoir in depression	0.1-0.8
	$\eta s_H/\eta s_D$	Outflow coefficient of slow flow reservoir	0.001-0.01
	$\eta f_H/\eta f_D$	Outflow coefficient of fast flow reservoir	0.01-0.15
	ke_H/ke_D	Exchange coefficient between slow and fast flow reservoirs (10^{-3})	0.1-1
	$\#\varphi_{HS}/\varphi_{DS}$	Exchange coefficient between active and passive storages for slow flow	0.1-0.5
	$\#\varphi_{HF}/\varphi_{DF}$	Exchange coefficient between active and passive storages for fast flow	
	$\#V_{HS,P}/V_{DS,P}$	Passive storage for slow flow (mm)	300-350
	$\#V_{HF,P}/V_{DF,P}$	Passive storage for fast flow (mm)	

Note: the upper and lower parameters and values in "*/*" represent those in hillslope and depression, respectively; the parameters indicated by "#" refer to those used for isotope concentration simulation. "-" represents not available.

4 Results

4.1 Performance of models during calibration and validation periods

The 30 optimal solutions and their means for the objective functions of KGE_q, KGE_c and $Abias_q$ are obtained from parameter calibration of 14 models as shown in Table 6 and Fig. 6. Most models obtain a higher KGE_q but a lower KGE_c, which was also reported by other studies (Soulsby et al., 2015; Dehaspe et al., 2018; Mudarra et al., 2019; Birkel et al., 2020). For the models incorporating 0-4 passive storages in Table 4, the accuracy of the simulated discharge and isotopic concentration does not increase with the number of passive stores. Comparatively, models *c*, *f* and *j* give higher mean values for both KGE_q (>0.65) and KGE_c (>0.55) (Table 6), and the models *c* and *f* also obtain a more constrained range of KGE_q and KGE_c from the 30 sets of optimal solutions (Fig. 6) in the calibration and validation periods. All of the three better performing models have a passive storage in the hillslope fast reservoir but do not incorporate any passive storage in the depression fast reservoir (see Table 4). This indicates that hillslope (fast) flow and isotope mixing catchment outlet discharge and isotopic concentration, are consistent with the inferences from the observational data analysis.

As an example, Figs. 7 and 8 show the outlet discharge and isotope (δD) variations, respectively, simulated by model *f*. Model *f* can generally capture the flood peaks (Fig. 7) and the isotope (δD) variations (Fig. 8). The average KGE_q and KGE_c from model *f* are higher than 0.59 in the calibration and validation periods, and $Abias_q$ is relatively small (Table 6). Fig. 9 shows that KGE_q is negatively correlated with KGE_c according to the 30 optimal solution sets by the NSGA-II algorithm. Therefore, the multi-objective calibration gives a trade-off solution pair of high values for both KGE_q and KGE_c for the calibrated model *f* as well as models *c* and *j*. The other models do not balance the trade-off between KGE_c against KGE_q as effectively. For example, model *n* with four passive storages obtains high KGE_q (>0.6) but low KGE_q (<0.3) (Table 6).

Table 6. Model performance based on the average of 30 optimal solution sets for each individual model structure

No. of Passive Storage	Model	Calibration			Validation		
		KGE_q	KGE_c	$Abias_q$	KGE_q	KGE_c	$Abias_q$
0	*a*	0.46	0.30	0.08	0.46	0.38	0.23
1	*b*	0.54	0.24	0.07	0.52	0.51	0.22
	c	**0.65**	**0.61**	**0.08**	**0.68**	**0.73**	**0.16**
	d	0.42	0.31	0.09	0.4	0.04	0.25

	e	0.52	0.45	0.09	0.53	0.22	0.18
2	***f***	**0.68**	**0.59**	**0.09**	**0.72**	**0.73**	**0.14**
	g	0.47	0.39	0.1	0.48	-0.12	0.19
	h	0.52	0.32	0.08	0.5	0.29	0.23
	i	0.65	0.15	0.07	0.67	0.5	0.12
3	***j***	**0.66**	**0.55**	**0.09**	**0.67**	**0.72**	**0.16**
	k	0.66	0.24	0.1	0.68	0.59	0.16
	l	0.63	0.21	0.08	0.64	0.32	0.14
	m	0.52	0.42	0.08	0.53	0.11	0.19
4	*n*	0.62	0.22	0.1	0.61	0.29	0.16

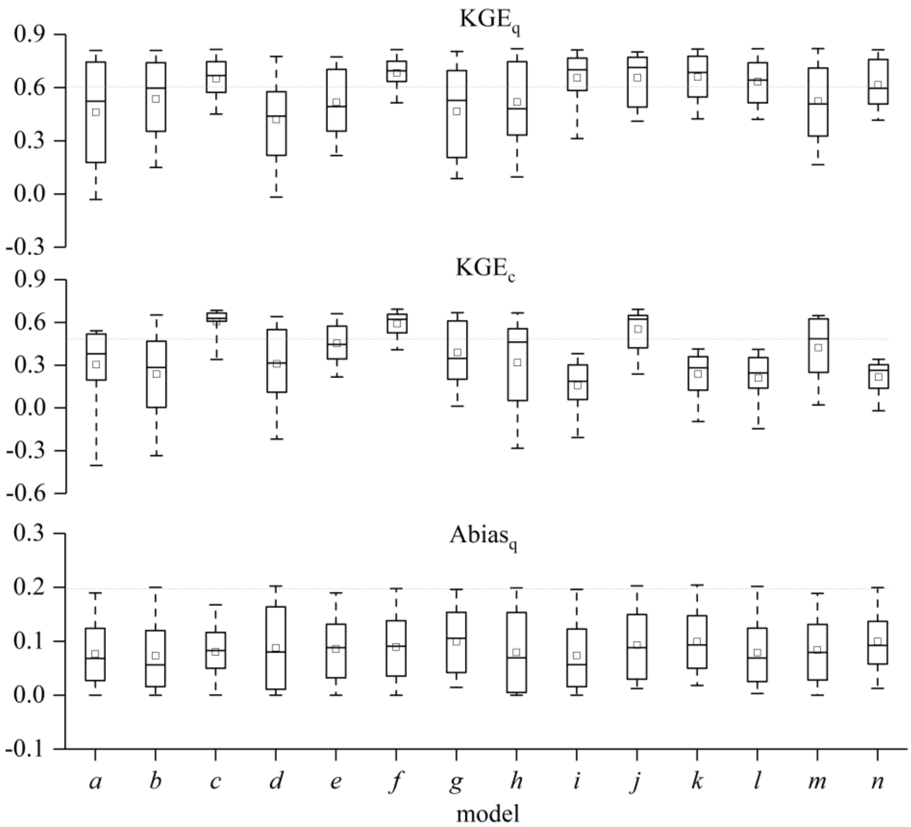

Figure 6. The box-plot of the 30 optimal solutions for the objective functions of KGE_q, KGE_c and $Abias_q$ obtained from parameter calibration of 14 models.

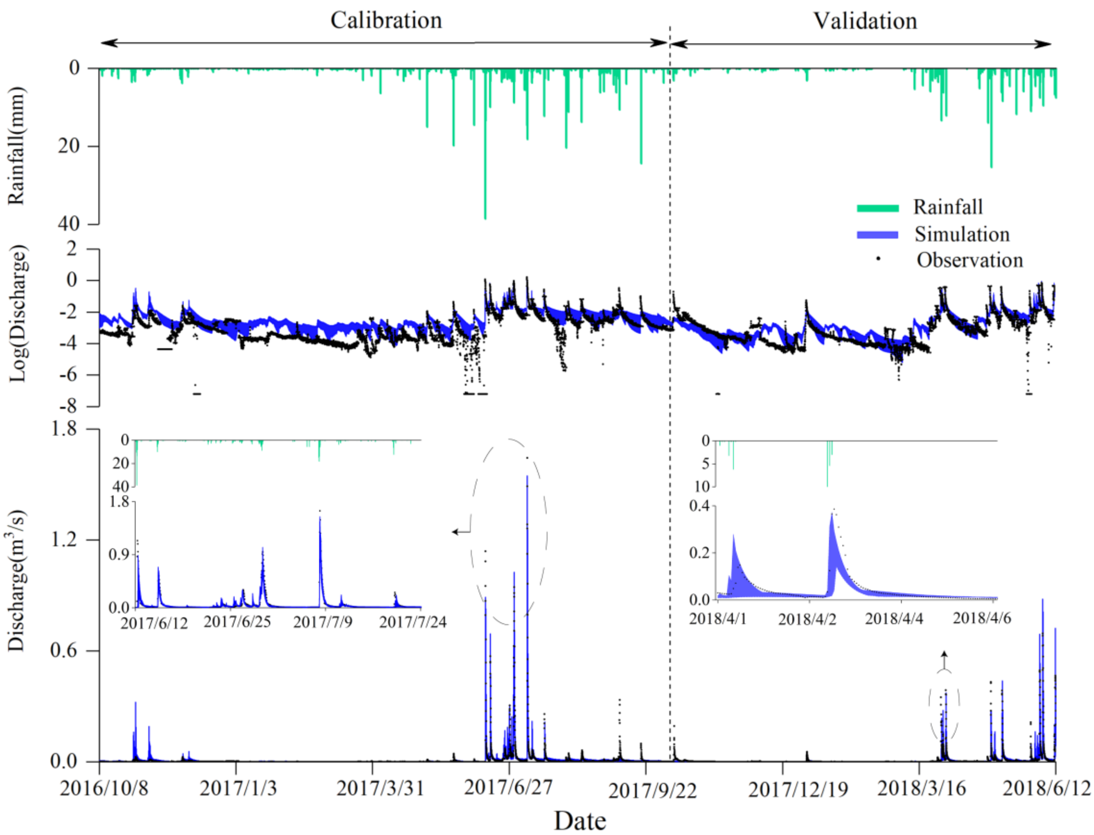

Figure 7. Simulated discharge concentrations of the 30 sets of optimal solutions by model *f* in calibration and validation periods. Note: The blue shades represent the simulated range of the 30 optimal solution sets; the black dots represent the observed discharge (the total of surface and subsurface discharge) at the catchment outlet.

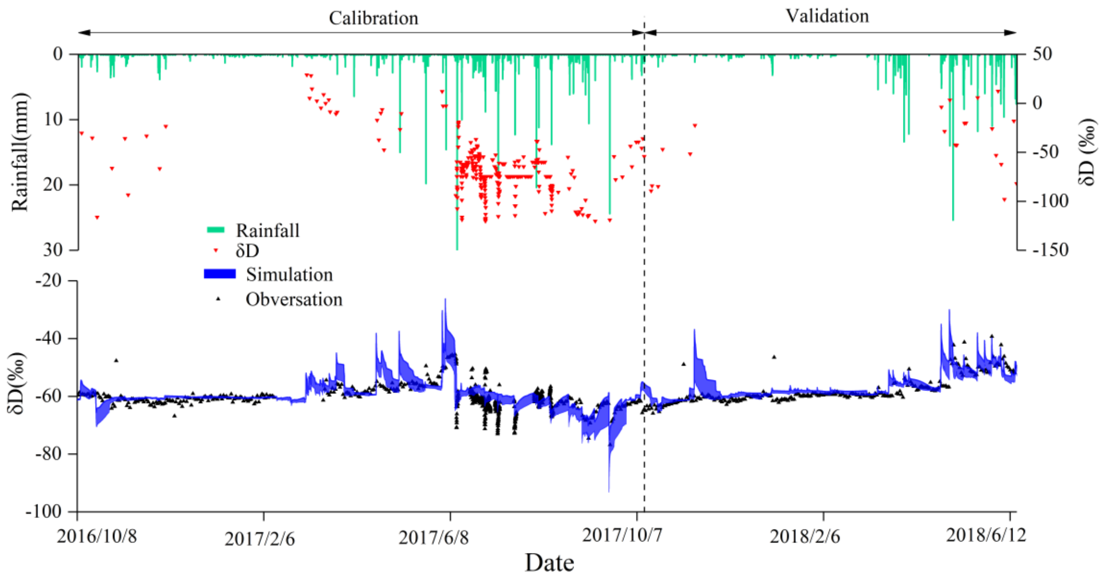

Figure 8. Simulated isotope concentrations of the 30 sets of optimal solutions by model *f* in calibration and validation periods. Note: The blue shades represent the simulated range of the 30 optimal solution sets; the black dots represent the observed isotope concentrations at the catchment outlet.

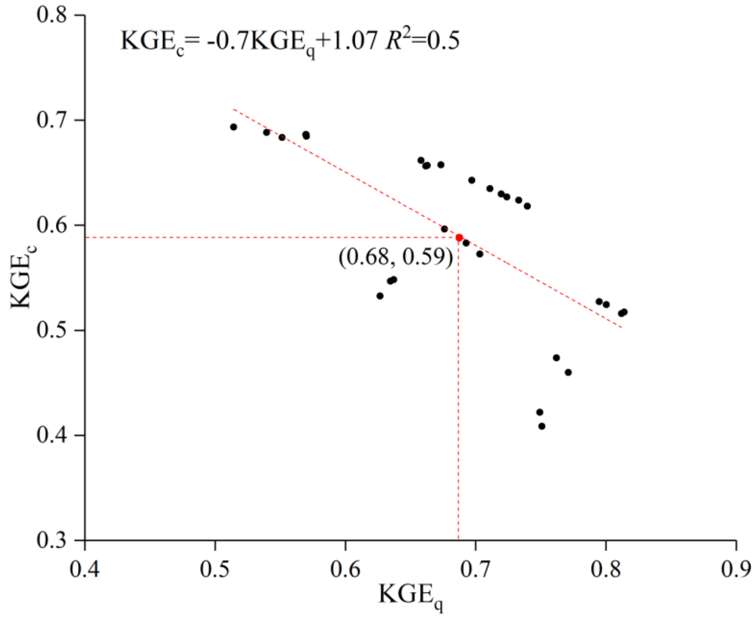

Figure 9. Relationship between KGE$_q$ and KGE$_c$ from the 30 optimal solution sets of model *f*.

4.2 Calibrated parameter values

The calibrated parameter values for the better performing models *c*, *f* and *j* are listed in Table 7. These parameter values reasonably delineate the hydrological features of karst landforms. For example, the calibrated *ks* ranges 0.13 - 0.24 in hillslope and depression units, suggesting about 76-87% of net precipitation recharging into fast flow reservoir through large fracture and sinkhole in terms of I_f/R=(1-α)P/R+(1-*ks*)α. This high percentage is consistent with the numerical results of Zhang et al. (2011) independently derived using a distributed model that takes account of the role of sinkholes in facilitating fast flow recharge into the aquifer in the studied catchment. Charlier et al.(2012) found that about 60% of recharge water entered the conduit network (fast channelized flow paths) in a small karst system in the French Jura mountains. Worthington et al. (2000) also revealed that more than 90% of fast flow component in four typical karst aquifers in Kentucky, USA. *wm* representing the soil moisture retention capacity ranges 52-58 mm for thin soils over hillslope, substantially smaller than 81-90 mm for thick soils over depression according to the calibrated results of the three better models. The outflow coefficient of the fast flow reservoir ηf (0.14-0.15/0.01-0.02 for the hillslope/depression) is much greater than that of slow flow reservoir ηs (0.002-0.004/0.003-0.005), especially for the hillslope unit. This suggests that fast flow discharge is much more sensitive to active storage variability than slow flow discharge since $Q=\eta s\times V$. In addition, the optimized ratio of hillslope slow flow contribution to depression slow flow r_{HD} is close for models *c* and *f* (0.37 and 0.39, respectively), which are smaller than 0.55 for model *j*. The larger r_{HD} value for model *j* means more hillslope slow flow allocation to the depression slow flow reservoir.

Table 7. The mean values of model parameters for the 30 optimal solution sets from the three better models

Zone	Parameter	Model *c*	Model *f*	Model *j*
Area	α_H/α_D	0.92/0.99	0.94/0.99	0.94/0.98
Unsaturated	kc_H/kc_D	1.14/1.08	1.12/1.04	1.17/1.15
	ks_H/ks_D	0.24/0.13	0.22/0.14	0.16/0.23
	b_H/b_D	0.14/0.24	0.11/0.15	0.24/0.15
	ls_H/ls_D	0.01/0.01	0.01/0.05	0.02/0.02
	wm_H/wm_D	58/90	56/82	52/81
	#$W_{H,P}/W_{D,P}$	547/534	535/509	528/517
Saturated	-/Vm	44	36	35
	r_{HD}	0.37	0.39	0.55
	$\eta s_H/\eta s_D$	0.002/0.005	0.004/0.003	0.003/0.004
	$\eta f_H/\eta f_D$	0.15/0.01	0.14/0.01	0.14/0.02
	ke_H/ke_D	0.2/0.3	0.2/0.3	0.3/0.5
	#$\varphi_{HS}/\varphi_{DS}$	-/-	0.18/-	0.22/0.29
	#$\varphi_{HF}/\varphi_{DF}$	0.25/-	0.26/-	0.19/-
	#$V_{HS,P}/V_{DS,P}$	-/-	316/-	331/323
	#$V_{HF,P}/V_{DF,P}$	322/-	325/-	334/-

Note: the upper and lower parameters and values in "*/*" represent those in hillslope and depression, respectively; the parameters indicated by "#" refer to those used for isotope concentration simulation. "-" represents not available in the models.

4.3 The effects of passive storage on simulated flow composition and isotopic concentration

We further compared the simulated flow components and their isotopic concentrations of the three better performing models (model *c*, *f* and *j* with passive stores 1-3 in Table 6). The results of model *a* without any passive store are also used as a benchmark for comparison. The partitioning of simulated outlet discharge by the four models is listed in Table 8. All three better models with passive stores set in the hillslope unit have a high proportion of discharge from the fast flow system, particularly in the hillslope unit. In the hillslope unit, model *a* obtains 79% of the fast flow component and 21% of the slow flow component, while the three better models with passive stores in the hillslope give a higher proportion of discharge from the fast flow system (87%). In the depression unit and catchment outlet, the simulated slow flow composition is slightly different, while the simulated proportions of the underground fast flow and surface flow are largely different in the three models. As shown in Table 8, model *f* gives 44% of surface stream flow and 56% of underground channel flow (the total of fast and slow flow), which are close to observed values at the surface stream (43%) and underground channel (57%) outlets. By contrast, models *a*, *c* and *j*, particularly model *a*, underestimate surface stream flow and overestimate underground channel flow.

The simulated isotope values of the flow components in the hillslope-depression-outlet continuum are listed in Table 9. Compared with model *a*, models *c*, *f* and *j* with passive storages increase isotope mixing and lead to a reduction of the δD variability (see the narrower range of δD for models *c*, *f* and *j* in Table 9). Meanwhile, as the number of passive storages increases in the models, the mixing of fast flow and slow flow is enhanced, leading to the mean δD values of slow flow approaching that of fast flow. Nevertheless, for the three better models, the strengthened mixing of slow flow only has a limited effect on the mean δD of fast flow as the mean δD of the catchment outlet flow is closer to that of fast flow. It further supports the hypothesis that hillslope fast flow dynamics control the catchment flow and isotopic concentration at the outlet.

Table 8. The proportions of flow components in the hillslope-depression-outlet continuum for the 30 optimal solution sets of the selected representative models during the study period (%)

No. of Passive storage	Model	Hillslope				Depression and catchment outlet					
		Slow flow		Fast flow		Slow flow		Fast flow		Surface flow	
		Range	Mean	Range	Mean	Range	Mean	Range	Mean	Range	Mean
0	*a*	4-34	21	66-96	79	4-20	12	36-80	56	0-57	32
1	*c*	6-27	13	73-94	87	3-15	8	39-60	54	27-57	38
2	*f*	6-27	13	73-94	87	4-15	8	37-58	48	31-59	44
3	*j*	6-29	13	71-94	87	4-17	9	38-74	51	20-56	40

Note: the total flow at the catchment outlet is the sum of slow flow, fast flow and surface flow.

Table 9. The simulated isotope values (‰) of flow components in the hillslope-depression-outlet continuum for the 30 optimal solution sets from the selected representative models during the study period

No. of Passive storage	Model	Hillslope				Depression and catchment outlet							
		Slow flow		Fast flow		Slow flow		Fast flow/Surface flow		Catchment outlet			
		Range	Mean	Range	Mean	Range	Mean	Range	Mean	Range (Sim.)	Mean (Sim.)	Range (Obs.)	Mean (Obs.)
0	*a*	-65.1- -35.8 (29.3)	-55.2	-102.6-9.8 (112.4)	-58.5	-73- -37 (36)	-56.4	-96.1- -8.9 (87.2)	-57.8	-93.3- -9.8 (103.6)	-57.5	-76.8- -39.3 (37.5)	-60.6
1	*c*	-70.7- -39.3 (31.4)	-56.3	-93-9.5 (102.5)	-59.4	-72.3- -41.9 (30.4)	-57.8	-84.3- -30.7 (53.6)	-59.4	-79.4- -31.6 (47.8)	-59.2		
2	*f*	-63.4- -44.8 (18.6)	-59.4	-95.2-10 (105.2)	-59.8	-68.4- -43.3 (25.1)	-58.9	-83.4- -31.5 (51.9)	-59.7	-80.9- -32.8 (48.1)	-59.6		
3	*j*	-61.8- -39.4 (22.4)	-59.3	-96.2-9.7 (105.9)	-59.5	-62.7- -49.8 (12.9)	-60	-85.1- -26.6 (58.5)	-59.2	-84.7- -28.8 (55.9)	-59.2		

Note: the number in blanket refers to the range of δD.

5. Discussion

5.1 Importance of passive storage for tracer-aided hydrological modeling

Involving passive storage for coupled flow-isotope model helped to improve the performance of the discharge simulations, whilst being able to capture tracer dynamics, which has been demonstrated by most previous studies (see Table 1). However, the exact configuration of how passive storage can be set in different positions for different models (Table 1), or even for a specific model. Taking the STARR model as an example, van Huijgevoort et al. (2016), Dehaspe et al. (2018) and Piovano et al. (2019) added two passive storages for the soil and groundwater stores, while Ala-Aho et al.(2017) and Piovano et al. (2020) only used a passive storage in the soil store. Of all the studies in Table 1, only Fenicia et al. (2008) and Birkel et al.(2011b) compared the simulation effects of model structures on discharge with and without passive storages.

Most previous studies have focused on non-karst catchments, and passive storages are usually represented in slow flow reservoirs (Hrachowitz et al., 2013; Yang et al., 2021; see Table 1). Birkel et al. (2011a) and Hrachowitz et al. (2013) suggested that this passive storage can be interpreted as soil moisture below field capacity or groundwater below the dynamic storage. For more complex model structures, delineating flow components and connections in heterogeneous landscape units usually requires more flow routing compartments and thus additional passive storages. For example, Capell et al. (2012) identified that only three passive storages were necessary for a tracer-aided model with four possible passive storages in upland and lowland units in the North Esk catchment in northeast Scotland. They found that passive storage in shallow zone for the upland unit was negligible as sufficient damping was available in the dynamic (active) storage.

Required model structures are usually more complex in karst catchments due to different conceptualisation of recharge and flow mechanisms. Most studies have demonstrated that the fast channelized flow paths control the sharp rise and decline of the hydrograph, and thus setting passive storage in fast flow reservoir can improve simulation accuracy of the catchment flow and tracer dynamics in karst catchments, particularly in cockpit karst landscapes. For example, Zhang et al. (2019) assumed that hillslope flow is rapid, and showed that directly setting a passive storage in the hillslope flow reservoir can successfully capture the dynamics of flow discharge and stable isotope in the same study catchment. Similarly, elsewhere, Chang et al. (2020) developed a model capturing the functioning of a dual flow system (fast flow and slow flow), showing that setting a passive storage in the fast flow reservoir can reproduce the dynamics of flow discharge and spring EC.

Our study was novel in comprehensively analyzing the functioning of alternative configurations of passive storage in a complex model structure for cockpit karst catchments, based on a comparison of the performances of 14 different models. We demonstrated through this comparison that adding passive storage in the fast flow reservoir in hillslope unit is more efficient for simulating flow components and isotope dynamics, with three alternative choices to set passive storages in our developed model. The most parsimonious model is to add a passive storage in the hillslope fast flow reservoir, as with model *c*. The "best" model is to add two passive storages in fast flow and slow reservoirs of the hillslope unit, as is the case with model *f*. This best model can appropriately estimate flow components in addition to the total discharge and isotope concentration at the catchment outlet. Adding an additional passive storage in the depression slow flow reservoir, such as model *j*, does not further substantially increase the simulation accuracy even though the model obtains higher KGE_q and KGE_c in Table 6.

5.2 The dominant transport processes: advection, dispersion or molecular diffusion?

Generally, the transport process is largely controlled by advection with the tracer travelling with water, though molecular diffusion in the slow velocity (or immobile) zone, and hydrodynamic dispersion in the fast velocity (or mobile) zone also contribute (Karadimitriou et al., 2016, Schumer et al., 2003, Wang et al., 2020). In karst flow systems, larger fracture and conduit media have permeability ranging across several orders of magnitude higher than matrix flow in micropores. In cockpit karst catchments, the hillslope unit has a higher flow velocity, but longer flow paths to the outlet. Tracers input farthest from the stream at the hillslope unit will undergo more dispersion (Kirchner et al., 2001). In our study catchment, the hillslope unit has a higher flow velocity as the outflow coefficient of fast flow in the modeled hillslope unit is much greater than that of the depression unit (Table 7) for the best performing models (*c*, *f*, and *j*). Meanwhile, configuring passive storage in the hillslope fast flow alone is sufficient to damp the δD variability effectively. This context, points to that hydrodynamic dispersion dominates the chemical mixing. Indeed, the dominance of hydrodynamic dispersion has been widely reported in flow-conductive (preferential flow) zones (Roubinet et al., 2012). For example, Zhao et al. (2019, 2021) used a transient storage model (TSM) to study the tailing of breakthrough curves (BTCs) of tracers in karst conduits, with experimental results suggesting that the dispersion coefficient was positively correlated with the flow velocity.

The mass exchange fluxes (EGM_F and EGM_S in Eqs. (11) and (12)) between active and passive storages are calculated in Table 10. The mass exchange flux of hillslope fast flow is greater than that of slow flow, and over 10 times larger than that of slow flow in depression unit. This result also supports that hillslope unit has stronger dispersion effects. Therefore, only when the functioning of the advection and dispersion of the hillslope unit is incorporated in the models, the stronger variations of discharge and isotopes can be better captured simultaneously.

Table 10. The simulated $|EGM|$ (m^3 ×‰) of flow components in the hillslope-depression-outlet continuum for the 30 optimal solution sets from the selected representative models during the study period

No. of Passive storage	Model	Hillslope				Depression and catchment outlet			
		Slow flow		Fast flow		Slow flow		Fast flow	
		Range	Mean	Range	Mean	Range	Mean	Range	Mean
1	*c*	-	-	0-42519	122	-	-	-	-
2	*f*	0-13776	35	0-51603	120	-	-	-	-
3	*j*	0-19816	42	0-46338	106	0-5773	10	-	-

Note: “-” represents not available.

5.3 Uncertainties of adding passive storage in the tracer-aided hydrological modeling

Our model uses a distribution curve of unsaturated storage capacity to describe the spatial heterogeneity of storage volumes, and fast flow and slow flow systems to conceptualise dual karst flow systems on a large scale (e.g. hillslope and depression units). Optimizing the number of storages balances the need to minimize model complexity and uncertainty, while still improving the simulation performance of both flow and tracers. Particularly for karst catchments, this optimization needs to be based on short-time-interval observation data, such as hourly data in our study catchment to capture the rapid hydrological response. Only such fine resolution data can capture the dramatic variability of the hydrograph and tracer dynamic, and thus can be used to successfully optimize the model structure. Nevertheless, the optimized passive storages and model structures are not unique, as the three better models with 1-3 passive storages performed similarly well in the study catchment, in terms of the catchment input-output responses.

These uncertainties imply that additional observations are needed to enhance our ability to constrain complex model structures and ranges of model parameters in karst catchments. These additional observations should include not only the catchment inputs - output responses, but also some key hydrological internal state components and their isotope concentrations, such as water fluxes and isotope transport in micropore, fracture and conduit media in karst catchment. Moreover, detailed observations of human activities are also important to reduce the modeling uncertainties. As shown in our study catchment, the depression is occupied by agricultural land. Groundwater pumping for agriculture use causes the sudden declines in streamflow and isotopic concentrations in June as shown in Fig. 7, which makes that the model overestimates low flow.

Our study catchment at Chenqi is broadly representative of extensive regions of headwater catchments in cockpit karst landscapes, and while the model parameters still need to be calibrated for specific catchments, the model is generic and transferable to other areas. The approach also has the potential to be used in upscaling to large catchments, though the model would then need to incorporate river and channel routing as these play an important role in regulating streamflow variations at larger scales.

6 Conclusions

In cockpit karst landscapes dominated by poljes and surrounding tower areas, depression areas are interconnected with isolated towers scattered throughout the terrain (Lyew et al., 2007). In this study, we developed and tested a coupled flow-tracer model for simulating discharge and isotope signatures for cockpit karst landscapes represented as a “hillslope-depression-outlet” continuum. We tested 14 simulation cases with alternative model structures by varying the number and configuration of passive storage in the fast/slow flow reservoirs of hillslope/depression units. The model structures and parameters were optimized using a multi-objective optimization algorithm to match the observed discharge and isotope dynamics in the Chenqi catchment of southwest China.

We found that for complex models developed for cockpit karst catchments, capturing the main hydrological flow paths and organising passive storages in relation to these flow paths can efficiently improve model performance. In the Chenqi catchment, the main hydrological pathways are hillslope flow and its connection with the catchment outlet. The models with 1-3 passive storages achieve similarly optimal results that are supported by the values of KGE_q, KGE_c and $Abias_q$. All three models have a passive storage in the dominant flow domain (hillslope fast flow).

The optimal model structure is supported by the simulated discharge and tracer dynamics. The hillslope fast flow system contributes about ~80% of the outlet discharge. The passive storages in the optimal models strengthen isotope mixing and thus constrain the δD and discharge variability. Further comparison of the simulated results by the three optimal models with 1-3 passive storages, showed the "best" model structure is to incorporate two passive storages in the fast and slow flow reservoirs of the hillslope unit. This best model can appropriately estimate flow components in addition to the total discharge and isotope fluctuations at the catchment outlet.

Characterizing the dynamics of flow paths and connections in complex geological settings karst landscapes is central to better understanding fluid flow and solute transport processes. This study provided evidence that the protection of hillslope environments is significant for the prevention of natural hazards, such as droughts, floods and contamination in karst landscapes.

Acknowledgment: This research was supported by the National Natural Science Foundation of China (42030506).

Data availability: The discharge and isotope data that support the findings of this study can be shared after the ending of our project according to the project executive policy. Anyone who would like to use the data can contact the corresponding author.

Code availability: The code that support the findings of this study is available from the corresponding author upon reasonable request.

Declaration of Competing Interest: I declare that neither I nor my co-authors have any competing interest.

References:

Adinehvand, R., Raeisi, E., Hartmann, A.: A step-wise semi-distributed simulation approach to characterize a karst aquifer and to support dam construction in a datascarce environment, J. Hydrol., 554, 470-481, https://doi.org/10.1016/j.jhydrol.2017.08.056, 2017.

Ala-Aho, P., Tetzlaff, D., Mcnamara, J.P., Laudon, H., Soulsby, C.: Using isotopes to constrain water flux and age estimates in snow-influenced catchments using the STARR (Spatially distributed Tracer-Aided Rainfall-Runoff) model, Hydrol. Earth Syst. Sci., 21, 5089-5110, https://doi.org/10.5194/hess-21-5089-2017, 2017.

Barnes, C. J., Bonell, M.: Application of unit hydrograph techniques to solute transport in catchments, Hydrol. Process., 10, 793-802, 1996.

Benettin, P., J. W. Kirchner, A. Rinaldo, G. Botter.: Modeling chloride transport using travel time distributions at Plynlimon, Wales, Water Resour. Res., 51, 3259-3276, https://doi.org/10.1002/2014WR016600, 2015.

Beven, K.: A manifesto for the equifinality thesis, J. Hydrol., 320, 18-36, https://doi.org/10.1016/j.jhydrol.2005.07.007, 2006.

Birkel, C., Tetzlaff, D., Dunn, S. M., Soulsby, C.: Using lumped conceptual rainfall-runoff models to simulate daily isotope variability with fractionation in a nested mesoscale catchment, Adv.Water Resour., 34, 383-394, https://doi.org/10.1016/j.advwatres.2010.12.006, 2011a.

Birkel, C., Soulsby, C., Tetzlaff, D.: Modelling catchment-scale water storage dynamics: reconciling dynamic storage with tracer-inferred passive storage, Hydrol. Process., 25, 3924-3936, https://doi.org/10.1002/hyp.8201, 2011b.

Birkel, C., Soulsby, C.: Advancing tracer-aided rainfall-runoff modelling: A review of progress, problems and unrealised potential, Hydrol. Process., 29, 5227-5240, https://doi.org/10.1002/hyp.10594, 2015.

Birkel, C., Soulsby, C., Tetzlaff, D.: Conceptual modelling to assess how the interplay of hydrological connectivity, catchment storage and tracer dynamics controls non-stationary water age estimates, Hydrol. Process., 29, 2956-2969, http://dx.doi.org/10.1002/hyp.10414, 2015.

Birkel, C., Duvert, C., Correa, A., Munksgaard, N. C., Maher, D. T., &Hutley, L. B.: Tracer-aided modeling in the low-relief, wet-dry tropics suggests water ages and

DOC export are driven by seasonal wetlands and deep groundwater, Water Resour. Res., 55, e2019WR026175, https://doi.org/10.1029/2019WR026175, 2020.

Capell, R., Tetzlaff, D., Soulsby, C.: Can time domain and source area tracers reduce uncertainty in rainfall-runoff models in larger heterogeneous catchments? Water Resour. Res., 48, W09544, https://doi.org/10.1029/2011wr011543, 2012.

Carey, S., Quinton, W.: Evaluating snowmelt runoff generation in a discontinuous permafrost catchment using stable isotope, hydrochemical and hydrometric data, Hydrol. Res., 35, 309-324, https://doi.org/10.2166/nh.2004.0023, 2004.

Chacha, N., Njau, K.N., Lugomela, G.V., Muzuka, A.N.N.: Groundwater age dating and recharge mechanism of Arusha aquifer, northern Tanzania: application of radioisotope and stable isotope techniques, Hydrogeol. J., 26, 2693-2706, https:// doi.org/10.1007/s10040-018-1832-0, 2018.

Chang, Y., Hartmann, A., Liu, L., Jiang, G., Wu, J.: Identifying more realistic model structures by electrical conductivity observations of the karst spring, Water Resour. Res., 57, e2020WR028587, https://doi.org/10.1029/2020WR028587, 2020.

Charlier, J.-B., Bertrand, C., Mudry, J.: Conceptual hydrogeological model of flow and transport of dissolved organic carbon in a small Jura karst system, J. Hydrol., 460, 52-64, http://dx.doi.org/10.1016/j.jhydrol.2012.06.043, 2012.

Chen, X., Zhang, Z., Soulsby, C., Cheng, Q., Binley, A., Jiang, R., Tao, M.: Characterizing the heterogeneity of karst critical zone and its hydrological function:

an integrated approach, Hydrol. Process., 2018, 32, 2932-2946, https://doi.org/10.1002/hyp.13232, 2018.

Cheng, Q., Chen, X., Tao, M., Binley, A.: Characterization of karst structures using quasi-3D electrical resistivity tomography, Environ. Earth Sci., 78, 285, https://doi.org/10.1007/s12665-019-8284-2, 2019.

Deb, K., Pratap, A., Agarwal, S., Meyarivan, T.: A fast and elitist multi-objective genetic algorithm: NSGA-II. IEEE Trans. Evol. Comput., 6, 182-197, https://doi.org/10.1109/4235.996017, 2002.

Dehaspe, J., Birkel, C., Tetzlaff, D., Sánchez-Murillo, R., Durá-Quesada, A.M., Soulsby, C.: Spatially-distributed tracer-aided modelling to explore water and isotope transport, storage and mixing in a pristine, humid tropical catchment, Hydrol. Process., 32, 3206-3224, https://doi.org/10.1002/hyp.13258, 2018.

Ding, H., Zhang, X., Chu, X., Wu, Q.: Simulation of groundwater dynamic response to hydrological factors in karst aquifer system, J. Hydrol., 587, 124995, https://doi.org/10.1016/j.jhydrol.2020.124995, 2020.

Delavau, C. J., Stadnyk, T., Holmes, T.: Examining the impacts of precipitation isotope input ($\delta_{18}O_{ppt}$) on distributed, tracer-aided hydrological modelling, Hydrol. Earth Syst. Sci., 21, 2595-2614, https://doi.org/10.5194/hess-21-2595-2017, 2017.

Dubois, E., Doummar, J., Pistre, S., Larocque, M.: Calibration of a lumped karst system model and application to the Qachqouch karst spring (Lebanon) under climate change conditions, Hydrol. Earth Syst. Sci., 24, 4275-4290, https://doi.org/10.5194/hess-24-4275-2020, 2020.

Dunn, S.M., Birkel, C., Soulsby, C., Tetzlaff, D.: Transit time distributions of a conceptual model: their characteristics and sensitivities, Hydrol. Process., 24, 1719-1729, https://doi.org/10.1002/hyp.7560, 2010.

Elghawi, R., Pekhazis, K., Doummar, J.: Multi-regression analysis between stable isotope composition and hydrochemical parameters in karst springs to provide insights into groundwater origin and subsurface processes: regional application to Lebanon, Environ. Earth Sci., 80, 1-21, https://doi.org/10.1007/s12665-021-09519-4, 2021.

Fenicia, F., Savenije, Hubert.H.G., Matgen, P., Pfister, L.: A comparison of alternative multiobjective calibration strategies for hydrological modeling, Water Resour. Res., 43, W03434, https://doi.org/10.1029/2006wr005098, 2007.

Fenicia, F., McDonnell, J. J., Savenije, H. H. G.: Learning from model improvement: on the contribution of complementary data to process understanding, Water Resour. Res., 44, W06419, https://doi.org/10.1029/2007WR006386, 2008.

Fenicia, F., Wrede, S., Kavetski, D., Pfister, L., Hoffmann, L., Savenije, H.H.G., McDonnell, J.J.: Assessing the impact of mixing assumptions on the estimation of streamwater mean residence time, Hydrol. Process., 24, 1730-1741, https://doi.org/10.1002/hyp.7595, 2010.

Freer, J., Beven, K., and Ambroise, B.: Bayesian estimation of uncertainty in runoff prediction and the value of data: An application of the GLUE approach, Water Resour. Res., 32, 2161-2173, https://doi.org/10.1029/96WR03723, 1996.

Hrachowitz, M., Savenije, H., Bogaard, T. A., Tetzlaff, D., Soulsby, C.: What can flux tracking teach us about water age distribution patterns and their temporal dynamics?, Hydrol. Earth Syst. Sci., 17, 533-564, https://doi.org/10.5194/hess-17-533-2013, 2013.

Hartmann, A., Barberá, J.A., Lange, J., Andreo, B., Weiler, M.: Progress in the hydrologic simulation of time variant recharge areas of karst systems-Exemplified at a karst spring in Southern Spain, Adv. Water Resour., 54, 149-160, https://doi.org/10.1016/j.advwatres.2013.01.010, 2013.

Husic, A., Fox, J., Adams, E., Ford, W., Agouridis, C., Currens, J., Backus, J.: Nitrate Pathways, processes, and timing in an agricul-tural karst system: Development and application of a numerical model, Water Resour. Res., 55, 2079-2103. https://doi.org/10.1029/2018WR023703, 2019.

Jeannin, P.Y., Artigue, G., Butscher, C., Chang, Y., Charlier, J.B., Duran, L., Gill, L., Hartmann, A., Johannet, A., Jourde, H., Kavousi, A., Liesch, T., Liu, Y., Lüthi, M., Malard, A., Mazzilli, N., Pardo-Igúzquiza, E., Thiéry, D., Reimann, T., Schuler, P., Wöhling, T., Wunsch, A.: Karst modelling challenge 1: Results of hydrological modelling, J. Hydrol., 600, 126508, https://doi.org/10.1016/j.jhydrol.2021.126508, 2021.

Jourde, H., Massei, N., Mazzilli, N., Binet, S., Batiot-Guilhe, C., Labat, D., Steinmann, M., Bailly-Comte, V., Seidel, J. L., Arfib, B., Charlier, J. B., Guinot, V., Jardani, A., Fournier, M., Aliouache, M., Babic, M., Bertrand, C., Brunet, P., Boyer, J. F., Bricquet, J. P., Camboulive, T., Carrière, S. D., Celle- Jeanton, H., Chalikakis, K., Chen, N., Cholet, C., Clauzon, V., Soglio, L. D., Danquigny, C., Défargue, C., Denimal, S., Emblanch, C., Hernandez, F., Gillon, M., Gutierrez, A., Sanchez, L. H., Hery, M., Houillon, N., Johannet, A., Jouves, J., Jozja, N., Ladouche, B., Leonardi, V., Lorette, G., Loup, C., Marchand, P., de Montety, V., Muller, R., Ollivier, C., Sivelle, V., Lastennet, R., Lecoq, N., Maréchal, J. C., Perotin, L., Perrin, J., Petre, M. A., Peyraube, N., Pistre, S., Plagnes, V., Probst, A., Probst, J. L., Simler, R., Stefani, V., Valdes-Lao, D., Viseur, S., Wang, X.: SNO KARST: A French Network of Observatories for the Multidisciplinary Study of Critical Zone Processes in Karst Watersheds and Aquifers, Vadose Zone J., 17, 180094, https://doi.org/10.2136/vzj2018.04.0094, 2018.

Lyew-Ayee, P., Viles, H, A., Tucker, G, E.: The use of GIS-based digital morphometric techniques in the study of cockpit karst, Earth Surf. Process. Landforms., 32, 165-179, https://doi.org/10.1002/esp.1399, 2007.

Mayer-Anhalt, L., Birkel, C., Sánchez-Murillo, R., Schulz, S.: Tracer-aided modelling reveals quick runoff generation and young streamflow ages in a tropical rainforest catchment, Hydrol. Process., 36, e14508, https://doi.org/10.1002/hyp.14508, 2022.

Mudarra, M., Hartmann, A., Andreo, B.: Combining experimental methods and modeling to quantify the complex recharge behavior of karst aquifers, Water Resour. Res., 55, 1384-1404, https://doi.org/10.1029/2017WR021819, 2019.

Neill, A. J., Tetzlaff, D., Strachan, N. J. C., and Soulsby, C.: To what extent does hydrological connectivity control dynamics of faecal indicator organisms in streams? Initial hypothesis testing using a tracer-aided model, J. Hydrol., 570, 423-435, https://doi.org/10.1016/j.jhydrol.2018.12.066, 2019.

Kirchner, J.W., Feng, X., Neal, C.: Catchment-scale advection and dispersion as a mechanism for fractal scaling in stream tracer concentrations, J. Hydrol., 254, 82-101, https://doi.org/10.1016/s0022-1694(01)00487-5, 2001.

Kling, H., Fuchs, M., Paulin, M.: Runoff conditions in the upper Danube basin under an ensemble of climate change scenarios, J. Hydrol., 424, 264-277, https://doi.org/10.1016/j.jhydrol.2012.01.011, 2012.

Kollat, J.B., Reed, P.M.: Comparing state-of-the-art evolutionary multi-objective algorithms for long-term groundwater monitoring design, Adv. Water Resour., 29, 792-807, https://doi.org/10.1016/j.advwatres.2005.07.010, 2006.

Karadimitriou, N.K., Joekar-Niasar, V., Babaei, M., Shore, C.A.: Critical Role of the Immobile Zone in Non-Fickian Two-Phase Transport: A New Paradigm. Environ. Sci. Technol., 50, 4384-4392, https://doi.org/10.1021/acs.est.5b05947, 2016.

Long, A.J., Putnam, L.D.: Linear model describing three components of flow in karst aquifers using ^{18}O data, J. Hydrol., 296, 254-270, https://doi.org/10.1016/j.jhydrol.2004.03.023, 2004.

Martínez‐Santos, P., Andreu, J.M.: Lumped and distributed approaches to model natural recharge in semiarid karst aquifers, J. Hydrol., 388, 389-398, https://doi.org/10.1016/j.jhydrol.2010.05.018, 2010.

Nan, Y., Tian, L., He, Z., Tian, F., Shao, L.: The value of water isotope data on improving process understanding in a glacierized catchment on the Tibetan Plateau, Hydrol. Earth Syst. Sci., 25, 3653-3673, https://doi.org/10.5194/hess-25-3653-2021, 2021.

Ollivier, C., Mazzilli, N., Olioso, A., Chalikakis, K., Carrière, S.D., Danquigny, C., Emblanch, C.: Karst recharge-discharge semi distributed model to assess spatial variability of flows, Sci. Total Environ., 703, 134368, https://doi.org/10.1016/j.scitotenv.2019.134368, 2020.

Page, T., Beven, K. J., Freer, J., Neal, C.: Modelling the chloride signal at Plynlimon, Wales, using a modified dynamic TOPMODEL incorporating conservative chemical mixing (with uncertainty), Hydrol. Process., 21, 292-307, https://doi.org/10.1002/hyp.6186, 2007.

Perrin, C., Michel, C., AndreÂassian, V.: Does a large number of parameters enhance model performance? Comparative assessment of common catchment model structures on 429 catchments, J. Hydrol., 242, 275-301, https://doi.org/10.1016/S0022-1694(00)00393-0, 2001.

Piovano, T. I., Tetzlaff, D., Carey, S. K., Shatilla, N. J., Smith, A., Soulsby, C.: Spatially distributed tracer-aided runoff modelling and dynamics of storage and water ages in a permafrost-influenced catchment, Hydrol. Earth Syst. Sci., 23, 2507-2523, https://doi.org/10.5194/hess-23-2507-2019, 2019.

Piovano, T. I., Tetzlaff, D., Maneta, M., Buttle, J. M., Carey, S. K., Laudon, H., McNamarah, J., Soulsby, C.: Contrasting storage-flux-age interactions revealed by catchment inter-comparison using a tracer-aided runoff model, J. Hydrol., 590, https://doi.org/10.1016/j.jhydrol.2020.125226, 2020.

Roubinet, D., Dreuzy, J., Tartakovsky, D.M.: Semi-analytical solutions for solute transport and exchange in fractured porous media, Water Resour. Res., 48, 273-279, https://doi.org/10.1029/2011WR011168, 2012.

Rodriguez, N. B., McGuire, K. J., Klaus, J.: Time-varying storage-Water age relationships in a catchment with a Mediterranean climate, Water Resour. Res., 54, 3988-4008, https://doi.org/10.1029/2017WR021964, 2018.

Son, K., Sivapalan, M.: Improving model structure and reducing parameter uncertainty in conceptual water balance models through the use of auxiliary data, Water Resour. Res., 43, W01415, https://doi.org/10.1029/2006wr005032, 2007.

Soulsby, C., Piegat, K., Seibert, J., Tetzlaff, D.: Catchment scale estimates of flow path partitioning and water storage based on transit time and runoff modelling, Hydrol. Process., 25, 3960-3976, https://doi.org/10.1002/hyp.8324, 2011.

Soulsby, C., C. Birkel, J. Geris, J. Dick, C. Tunaley, D, Tetzlaff.: Stream water age distributions controlled by storage dynamics and nonlinear hydrologic connectivity: Modeling with high-resolution isotope data, Water Resour. Res., 51, 7759-7776, https://doi.org/10.1002/2015WR017888, 2015.

Sprenger, M., Tetzlaff, D., Soulsby, C.: Soil water stable isotopes reveal evaporation dynamics at the soil-plant-atmosphere interface of the critical zone, Hydrol. Earth Syst. Sci., 21, 3839-3858, https://doi.org/10.5194/hess-21-3839-2017, 2017.

Sprenger, M., D. Tetzlaff, J. Buttle, H. Laudon, H. Leistert, C.P.J. Mitchell, J. Snelgrove, M. Weiler, and C. Soulsby.: Measuring and modeling stable isotopes of mobile and bulk soil water, Vadose Zone J., 17, 170149, https://doi.org/10.2136/vzj2017.08.0149, 2018.

Schumer, R., Benson, D.A., Meerschaert, M.M., Baeumer, B.: Fractal mobile/immobile solute transport, Water Resour. Res., 39, 1296, https://doi.org/10.1029/2003WR002141, 2003.

van Huijgevoort, M. H. J., Tetzlaff, D., Sutanudjaja, E. H., Soulsby, C.: Using high resolution tracer data to constrain water storage, flux and age estimates in a spatially distributed rainfall-runoff model, Hydrol. Process., 30, 4761-4778, https://doi.org/10.1002/hyp.10902, 2016.

Wang, L., Cardenas, M. B., Zhou, J.Q., Ketcham, R. A.: The complexity of nonlinear flow and non-Fickian transport in fractures driven by three-dimensional recirculation zones, J. Geophys. Res.-Solid Earth., 125, e2020JB020028, https://doi.org/10.1029/2020JB020028, 2020.

White, W.B.: A brief history of karst hydrogeology: contributions of the NSS, J. Cave Karst Stud., 69, 13-26, 2007.

Worthington, S.R.H., Davies, G.J., Ford, D.C., Sasowsky I.D.(eds), Wicks C.M.(des): Matrix, fracture and channel components of storage and flow in a Paleozoic limestone aquifer. Groundwater flow and contaminant transport in carbonate aquifers. Balkema Publications, Rotterdam, The Netherlands, 2000.

Worthington S.R.H.: Diagnostic hydrogeologic characteristics of a karst aquifer (Kentucky, USA), Hydrogeol. J., 17, 1665-1678, https://doi.org/10.1007/s10040-009-0489-0, 2009.

Wunsch, A., Liesch, T., Cinkus, G., Ravbar, N., Chen, Z., Mazzilli, N., Jourde, H., and Goldscheider, N.: Karst spring discharge modeling based on deep learning using spatially distributed input data, Hydrol. Earth Syst. Sci., 26, 2405-2430, https://doi.org/10.5194/hess-26-2405-2022, 2022.

Xu, C., Xu, X., Liu, M., Li, Z., Zhang, Y., Zhu, J., Wang, K., Chen, X., Zhang, Z., Peng, T.: An improved optimization scheme for representing hillslopes and depressions in karst hydrology, Water Resour. Res., 56, e2019WR026038, https://doi.org/10.1029/2019WR026038, 2020.

Xue, B., Chen, X., Zhang, Z., Cheng, Q.: A Semi-distributed Karst Hydrological Model Considering the Hydraulic Connection Between Hillslope and Depression: a case Study in Chenqi Catchment, China Rural Water And Hydropower., 437, 1-5, 2019. (In Chinese)

Yang, X., Tetzlaff, D., Soulsby, C., Smith, A., Borchardt, D.: Catchment functioning under prolonged drought stress: tracer-aided ecohydrological modeling in an intensively managed agricultural catchment, Water Resour. Res., 57, e2020WR029094, https://doi.org/10.1029/2020WR029094, 2021.

Zhang, Z., Chen, X., Ghadouani, A., Peng, S.: Modelling hydrological processes influenced by soil, rock and vegetation in a small karst basin of southwest China, Hydrol. Process., 25, 2456-2470, https://doi.org/10.1002/hyp.8022, 2011.

Zhang, R., Chen, X., Zhang, Z., Soulsby, C.: Using hysteretic behavior and hydrograph classification to identify hydrological function across the "hillslope-depression-stream" continuum in a karst catchment, Hydrol. Process., 34, 3464-3480, https://doi.org/10.1002/hyp.13793, 2020a.

Zhang, Z., Chen, X., Cheng, Q., Soulsby, C.: Storage dynamics, hydrological connectivity and flux ages in a karst catchment: conceptual modelling using stable isotopes, Hydrol. Earth Syst. Sci., 23, 51-71, https://doi.org/10.5194/hess-23-51-2019, 2019.

Zhang, Z., Chen, X., Cheng, Q., Soulsby, C.: Characterizing the variability of transit time distributions and young water fractions in karst catchments using flux tracking. Hydrol. Process., 34, 15, https://doi.org/10.1002/hyp.13829, 2020b.

Zhao, R.J.: The xinanjiang model applied in china. J. Hydrol., 135, 371-381, https://doi.org/10.1016/0022-1694(92)90096-E, 1992.

Zhao, X., Chang, Y., Wu, J., Xue, X.: Effects of flow rate variation on solute transport in a karst conduit with a pool, Environ. Earth Sci., 78, 237, https://doi.org/10.1007/s12665-019-8243-y, 2019.

Zhao, X., Chang, Y., Wu, J., Li, Q., Cao, Z.: Investigating the relationships between parameters in the transient storage model and the pool volume in karst conduits through tracer experiments, J. Hydrol., 593, 125825, https://doi.org/10.1016/j.jhydrol.2020.125825, 2021.